JACC: BASIC TO TRANSLATIONAL SCIENCE VOL. 11, NO. 4, 2026

ORIGINAL RESEARCH - PRECLINICAL

eNOS Uncoupling-ER Stress-Mitochondrial Dysfunction Axis in the Development of Pulmonary Hypertension

Priya Murugesan, PhD,[a,b,*] Yunxia Zhang, MD, PhD,[c,*] Meng Zhang, MD, PhD,[c] Yixuan Zhang, PhD,[a,b] Hua Cai, MD, PhD[a,b]

VISUAL ABSTRACT

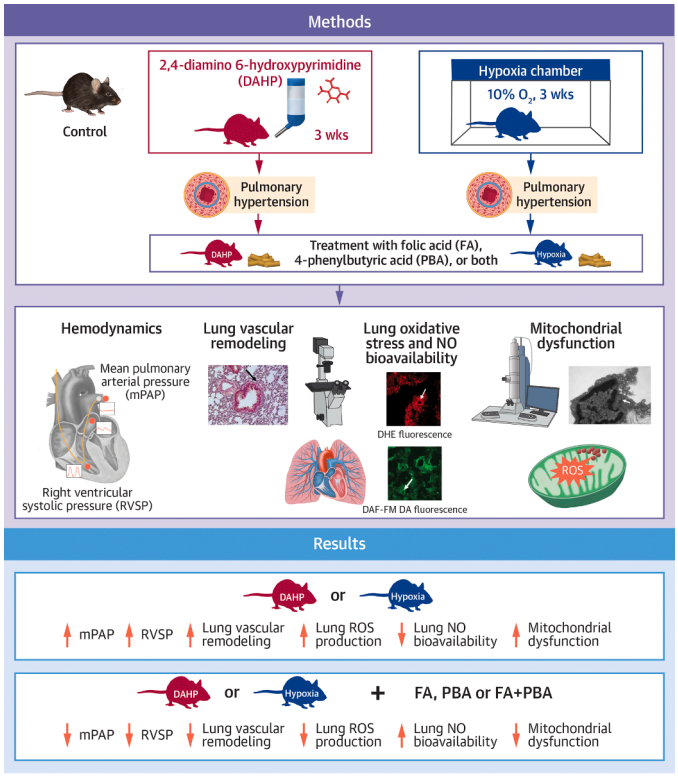

Murugesan P, et al. JACC Basic Transl Sci. 2026;11(4):101512.

HIGHLIGHTS

- **Our data identify a novel eNOS uncoupling-ER stress-mitochondrial dysfunction signaling axis in the pathogenesis of PH.**
- **FA (attenuating eNOS uncoupling) or PBA (abrogating ER stress) markedly alleviated mPAP/RVSP, vascular remodeling, total and mitochondrial superoxide production, and eNOS uncoupling, while preserving NO bioavailability.**
- **MitoTempo to scavenge mitochondrial ROS abolished molecular and pathophysiological features of PH. FA, PBA, or combination attenuated mitochondrial swelling and distortion of mitochondrial cristae.**
- **Our data for the first time reveal a novel eNOS uncoupling driven signaling axis in mediating PH, targetable for novel therapeutics effective in alleviating pathophysiological processes of the disease but not just the clinical symptoms, which is necessary to stop disease progression to save lives.**

From the [a]Division of Molecular Medicine, Department of Anesthesiology, David Geffen School of Medicine, University of California Los Angeles, Los Angeles, California, USA; [b]Division of Cardiology, Department of Medicine, David Geffen School of Medicine, University of California Los Angeles, Los Angeles, California, USA; and the [c]Department of Pulmonary Medicine, Capital Medical University, Beijing, China. *These authors contributed equally to this work.
The authors attest they are in compliance with human studies committees and animal welfare regulations of the authors' institutions and Food and Drug Administration guidelines, including patient consent where appropriate. For more information, visit the Author Center.

Manuscript received September 30, 2025; revised manuscript received January 22, 2026, accepted January 26, 2026.

ISSN 2452-302X https://doi.org/10.1016/j.jacbts.2026.101512

JACC: BASIC TO TRANSLATIONAL SCIENCE VOL. 11, NO. 4, 2026
APRIL 2026:101512

ABBREVIATIONS AND ACRONYMS

4-PBA = 4-phenylbutyric acid

DAF-FM DA = 4-amino-5-methylamino-2′,7′-difluorofluorescein diacetate

DAHP = 2,4-diamino 6-hydroxypyrimidine

DHE = dihydroethidium

EM = electron microscopy

eNOS = endothelial nitric oxide synthase

ER = endoplasmic reticulum

ESR = electron spin resonance

FA = folic acid

L-NAME = L-NG-nitro arginine methyl ester

mPAP = mean pulmonary arterial pressure

OCT = optimal cutting temperature

PAECs = pulmonary artery endothelial cells

PAH = pulmonary arterial hypertension

PBS = phosphate-buffered saline

PBST = phosphate-buffered saline with 0.1% Tween

PCNA = proliferating cell nuclear antigen

PDI = protein disulfide isomerase

PH = pulmonary hypertension

ROS = reactive oxygen species

RVSP = right ventricular systolic pressure

SMA = smooth muscle α-actin

SUMMARY

Pulmonary hypertension (PH) was induced by 2,4-diamino 6-hydroxypyrimidine or hypoxia exposure. Remarkably, folic acid (attenuating endothelial nitric oxide synthase [eNOS] uncoupling) or phenylbutyric acid (abrogating endoplasmic reticulum stress) markedly alleviated mean pulmonary arterial pressure /right ventricular systolic pressure, vascular remodeling, total and mitochondrial superoxide production, and eNOS uncoupling, while preserving NO bioavailability. MitoTempo to scavenge mitochondrial reactive oxygen species abolished molecular and pathophysiological features of PH. Folic acid, phenylbutyric acid, or combination attenuated mitochondrial swelling and distortion of mitochondrial cristae. Using 2,4-diamino 6-hydroxypyrimidine increased total and mitochondrial superoxide production in pulmonary artery endothelial cells. Our data for the first time establish a novel eNOS uncoupling/endoplasmic reticulum stress/mitochondrial dysfunction signaling axis in mediating PH, which are targetable for novel therapeutics.

Pulmonary hypertension (PH) is a condition characterized by progressive remodeling and narrowing of pulmonary arteries and consequent elevation in pulmonary blood pressure that can lead to right heart failure and death.[1] PH is defined as a mean pulmonary arterial pressure (mPAP) >20 mm Hg at rest, per the Seventh World Symposium on Pulmonary Hypertension in 2018,[2] and >25 mm Hg at rest per the guidelines issued by the European Society of Cardiology/European Respiratory Society in 2015.[3] The pathogenesis of PH involves a complex and multifactorial process. Endothelial dysfunction has been shown to play an important role in mediating remodeling of the pulmonary vasculature. It is logical to design new treatments to ameliorate endothelial dysfunction and endothelial cell proliferation at later stage to reduce medial thickening and smooth muscle cell hypertrophy, formation of intimal lesions, and fibrosis as seen in the pulmonary vasculature of patients with pulmonary arterial hypertension (PAH).[4] Major therapeutic advances have been made in the past 2 decades, with the introduction of novel compounds that target the 3 key pathways involved in the development and progression of PAH, namely: the endothelin, nitric oxide (NO), and prostacyclin pathways.[5]

Endothelial nitric oxide synthase (eNOS) is a key enzyme in producing NO to modulate pulmonary vascular homeostasis and protect against pulmonary vascular remodeling.[6] It is a potent vasodilator produced locally in the lung and mediates vascular smooth muscle relaxation.[7] It also inhibits vascular smooth muscle cell proliferation and migration. The pulsed delivery of NO was shown to be as effective as continuous therapy in reducing mean pulmonary artery pressure and pulmonary vascular resistance.[8] Patients who receive inhaled NO have a shortened hospital stay, fewer days of ventilation, and fewer hours on extracorporeal membrane oxygenation.[9] Therapies targeting the NO-cyclic guanosine monophosphate signaling pathway such as nitrovasodilators (inhaled NO), phosphodiesterase 5 inhibitors (sildenafil and tadalafil),[10] and cyclic guanosine monophosphate agonists (riociguat)[11-13] have been used as pulmonary vasodilators to improve hemodynamics, functional status, and symptomatology. For example, the COMPASS-2 (Combination of Bosentan and Sildenafil versus Sildenafil Monotherapy on Pulmonary Arterial Hypertension) trial was able to show an improvement in the 6-minute walk test after 16 weeks of treatment but failed to delay the time to the first morbidity/mortality event.[14] However, meta-analysis of data from studies that involve combination therapy indicate that this approach is effective, as detailed in this treatment of PAH.[15] Because endothelial dysfunction may represent the initiating step of idiopathic PAH, we hypothesize that direct depletion of eNOS coupling activity/uncoupling of eNOS is causal of PH. We have established a novel murine model of PH that is more human like by directly uncoupling eNOS with DAHP,[16] and in the present study, we aimed to examine signaling cascades downstream of uncoupled eNOS in driving PH development using this new model as well as the classical model of hypoxia-induced PH.

Recent studies have implicated an intermediate role of endoplasmic reticulum (ER) stress in the

pathogenesis of PH. ER stress is referred to as accumulation of unfolded and/or misfolded proteins in the ER. Newly synthesized proteins translocate to the ER lumen, where protein molecules undergo folding to form 3-dimensional structures. Interestingly, it has been shown that stressed ER produces reactive oxygen species (ROS) in the cardiovascular system.[17-19] As to studies in PH, administration of ER stress inhibitor 4-phenylbutyric acid (4-PBA) significantly attenuated right ventricular systolic pressure (RVSP) and prevented RV remodeling, which correlated with suppressed expression of the ER stress markers in lung tissues.[20] The mitochondrion is an essential organelle crucial in energy generation and regulation of calcium homeostasis.[21] Mitochondrial dysfunction has also been shown to generate excessive ROS.[22] Furthermore, several lines of evidence have shown that mitochondrial dysfunction occurs in PH through increased ROS production.[23-26] The ER and mitochondria are closely connected organelles within cells. ER stress contributes to mitochondrial dysfunction, which in turn facilitates cardiac injury.[27] We have shown that aggravated eNOS uncoupling activity leads to mitochondrial dysfunction, contributing to the development of abdominal aortic aneurysm and hypertension.[28,29] However, the inter-relationships among eNOS uncoupling, ER stress, and mitochondrial dysfunction, particularly during the development of PH, remain completely unknown. Therefore, we hypothesize that the initial activation of eNOS uncoupling can lead to oxidative induction of ER stress and subsequent mitochondrial dysfunction to induce PH.

Our data indicate that in 2,4-diamino 6-hydroxypyrimidine (DAHP, an inhibitor of H_4B synthetic enzyme GCH1) and hypoxia-induced PH models, uncoupling of eNOS induced ER stress and subsequent mitochondrial dysfunction, contributing to the development of PH. Recoupling of eNOS with folic acid (FA), preservation of ER function with PBA, or treatment with MitoTempo to scavenge mitochondrial ROS, attenuated elevations in mPAP and RVSP, decreased superoxide production, reduced vascular remodeling, and restored NO availability while preventing ER stress and mitochondrial dysfunction in both DAHP- and hypoxia-induced PH mice. FA or PBA attenuated increased expression of ER stress marker protein disulfide isomerase (PDI) in PH, indicating an upstream role of eNOS uncoupling in mediating ER stress, FA or PBA also abrogated mitochondrial ROS production and mitochondrial swelling activity, indicating that mitochondrial dysfunction is downstream of uncoupled eNOS and ER stress. In addition, electron microscopy (EM) data demonstrate that there was a robust distortion of cristae structure of mitochondria in both DAHP and hypoxic models of PH, which was alleviated by treatment with FA or PBA. Further, PBA treatment attenuated superoxide production, eNOS uncoupling activity, and dysfunctional mitochondria, indicating benefits of ER stress correction by shutting down ER stress-eNOS uncoupling feed-forward mechanism. In addition, DAHP induced significant up-regulation in ER stress marker PDI, eNOS uncoupling activity, and mitochondrial ROS production, indicating downstream role of ER stress following eNOS uncoupling in DAHP-treated pulmonary artery endothelial cells (PAECs). These data clearly indicate a novel signaling axis of eNOS uncoupling/ER stress/mitochondrial dysfunction in the pathogenesis of PH, targeting of which may promote development of novel therapeutics.

METHODS

ANIMALS AND PROTOCOLS ESTABLISHING PH. All animal experiments were approved by the University of California Los Angeles Institutional Animal Care and Use Committee and the Animal Ethics Committee of the China-Japan Friendship Hospital. The C57BL/6 male mice (8-10 weeks old) were purchased from Charles River Laboratories. The animals were housed under international standard laboratory conditions of light (12-hour light-dark cycle), temperature (22 ± 3 °C) and relative humidity of 60 ± 5% with good ventilation. Two murine models of PH, the newly established DAHP (#81260, Cayman) and the classical hypoxia models, were used in this study[16] to identify novel molecular mechanisms underlying development of PH. For the experiments of DAHP induction, mice were divided into 5 groups as the followings: a normal control group (n = 4); a DAHP group to directly provoke uncoupling of eNOS in the endothelium (DAHP, 10 mmol/L, n = 7); a DAHP group treated with FA (DAHP + FA, n = 5); a DAHP group treated with 4-PBA (DAHP + PBA, n = 5); and a DAHP group treated with both FA and 4-PBA (DAHP + PBA + FA, n = 4-5). Control group was given standard mouse chow and regular water, whereas the latter 4 groups were treated with DAHP in drinking water (10 mmol/L, refreshed every 2 days) for 3 weeks with or without FA, PBA, or FA + PBA. For the experiments using hypoxia model, mice were randomly divided into 5 groups: a normal control group (n = 4); a hypoxia group (n = 7-8); a hypoxia group treated with FA to attenuate uncoupling of eNOS (Hypoxia + FA, 15 mg/kg/d customized diet, n = 5-6)[26,30-35]; a hypoxia group treated with 4-PBA to

attenuate ER stress (Hypoxia + PBA, 1 g/kg/d, n = 5-7); and a hypoxia group treated with both FA and 4-PBA (Hypoxia + FA + PBA, n = 7). The control group was kept under room air, and the latter 4 groups were kept under hypoxic condition (normobaric 10% O_2, in 5% CO_2 balanced with 90% N_2) using hypoxic chamber for 3 weeks. All of the special chow diets were made in house at University of California Los Angeles or customized by Beijing HFK Bioscience Co, Ltd. All mice were fed ad libitum, and mouse chow was replaced every 2 days.

HEMODYNAMIC ANALYSES. Hemodynamic parameters of mPAP, RVSP, and left ventricular systolic pressure were determined using an open chest method in mice anesthetized with intraperitoneal injection of pentobarbital at 60 mg/kg. The animals were intratracheally intubated and connected to a respirator to maintain breathing (95% O_2-5% CO_2). The chest was opened, and the RV was localized. A 1.4-F catheter (mikro-tip catheter-transducer; model SPR-671, Millar Instruments) was introduced using a 20-G needle. The RVSP, left ventricular systolic pressure, and mPAP were recorded using a Power Lab data acquisition system (AD Instruments Inc).

TISSUE HARVEST AND HISTOLOGIC ANALYSES. Middle region of the left lung tissues of all mice were used for paraffin embedding, sectioning, and histologic analyses. In brief, the lung tissues were stored in 4% paraformaldehyde for a day, followed by a 24-hour incubation in 10% sucrose solution. After being fixed for 48 hours, the tissues were embedded in paraffin, cut into 5-μm thick sections, and stained with hematoxylin and eosin. Structural remodeling of the pulmonary arterioles was assessed by imaging of the pulmonary arterioles using Nikon A1R Confocal Microscope. Measurements of percentage of medial wall thickness of pulmonary arterioles with diameter size under 200 μm were analyzed using ImageJ software (National Institutes of Health). For each pulmonary arteriole, medial wall thickness was calculated as percentage of wall thickness = (wall thickness × 2/external diameter) × 100.

IMMUNOHISTOCHEMISTRY. Formalin-fixed, paraffin-embedded lung tissue sections were used for immunohistochemical staining. Paraffin was removed by washing with xylene and then rehydrated with descending concentrations of ethanol. Antigen retrieval was performed by immersing the sections in an antigen retrieval buffer (10 μmol/L citric acid, PH 5.0) at 98.5 °C for 20 minutes. Sections were washed in phosphate-buffered saline (PBS), followed by a 30-minute incubation in 0.3% hydrogen peroxide diluted in phosphate-buffered saline with 0.1% Tween (PBST). Then sections were blocked with 10% normal goat serum in PBST at room temperature for 30 minutes, and then incubated with anti-α-actin (ab5694, 1:400, Abcam), anti-proliferating cell nuclear antigen (anti-PCNA, ab18197, 1:800, Abcam), anti-protein disulfide isomerase-A1 (anti-PDI, ab2792, 1:200, Abcam), and subjected to the Real EnVision Detection System (K5007, DAKO) for detection of corresponding proteins. The images were taken by OLYMPUS BX 53 and analyzed and quantified using ImageJ program.

DETERMINATION OF TOTAL SUPEROXIDE PRODUCTION, eNOS UNCOUPLING ACTIVITY, AND MITOCHONDRIAL ROS PRODUCTION USING FLUORESCENT PROBES. Total superoxide production in the lung tissues was determined using dihydroethidium (DHE) fluorescent imaging. Superior lobes from the right lungs were freshly isolated and embedded in optimal cutting temperature (OCT) compound (Fisher HealthCare). The frozen blocks were then cut into 5-μm cryostat sections. To determine eNOS uncoupling activity, freshly prepared OCT sections were incubated with DHE solution (2 μmol/L, #D7008, Sigma) in the dark at 37 °C for 30 minutes in the presence or absence of NOS inhibitor L-NG-nitro arginine methyl ester (L-NAME; 100 μmol/L). The fluorescent intensity was captured using a Nikon A1R Confocal Microscope at excitation and emission wavelengths of 495 and 515 nm, respectively, and the images were quantified using ImageJ software.

DETERMINATION OF TOTAL SUPEROXIDE PRODUCTION AND eNOS UNCOUPLING ACTIVITY USING ESR. Superoxide levels in the lung tissues were specifically determined using electron spin resonance (ESR) as we previously published.[28,30,32,36-40] In brief, freshly isolated lung tissues were homogenized on ice in lysis buffer containing 1:100 protease inhibitor cocktail, and centrifuged at 12,000*g* for 10 minutes. Protein content of the supernatant was determined using a protein assay kit (Bio-Rad). Five to 10 μg of protein was mixed with ice-cold and nitrogen-bubbled Krebs/4-(2-hydroxyethyl)piperazine-1-ethanesulfonic acid buffer containing diethyldithiocarbamic acid (5 μmol/L), deferoxamine (25 μmol/L), and the superoxide-specific spin trap methoxycarbonyl-2,2,5,5-tetramethylpyrrolidine (500 μmol/L, Axxora). The mixture was then loaded into a glass capillary (Kimble), and assayed using the ESR spectrometer (eScan, Bruker) for superoxide production. A second measurement was taken with the addition of polyethylene glycol-conjugated superoxide dismutase (20 U/mL) to calculate SOD-inhibitable fraction of the ESR signal for specific

superoxide production. For assessment of eNOS uncoupling activity, a third measurement was made with the addition of L-NAME (10 μmol/L, Cayman). The rate of superoxide production was presented as micromolar/min/mg of protein after normalizing quantitative ESR signals to protein contents.

DETERMINATION OF INTRACELLULAR NO LEVELS BY DAF-FM FLUORESCENT IMAGING. The 4-amino-5-methylamino-2′,7′-difluorofluorescein diacetate (DAF-FM DA) is a reagent used to measure intracellular levels of NO. To measure NO levels in the lung tissues, freshly prepared 5-μm lung tissue sections were incubated with 20 μmol/L DAF-FM DA (D-23844, Molecular Probes) at 37 °C for 20 minutes in the dark. After washing with PBS for 3 times, the sections were cover slipped. The mean fluorescent intensity was captured using a Nikon A1R Confocal Microscope at excitation and emission wavelengths of 495 and 515 nm, respectively, and the images were quantified using ImageJ software.

DETERMINATION OF MITOCHONDRIAL ROS PRODUCTION USING MitoSOX FLUORESCENT IMAGING. In parallel experiments, freshly prepared 5-μm OCT lung sections were incubated in MitoSOX Red (5 μmol/L, M36008, Invitrogen) in the dark at 37 °C for 10 minutes to measure mitochondrial superoxide production specifically. After incubation, the fluorescent dye was washed away and the sections were visualized using a Nikon A1R Confocal Microscope. All images were analyzed and quantified using ImageJ software. Mean fluorescent intensity was taken from 6 images for each group.

PAEC CULTURE AND DAHP STIMULATION. PAECs (#2535, Lonza) between the fourth and seventh passages were cultured in the complete EGM-2 bullet Kit medium (CC-2535, Lonza) in humidified incubators at the conditions of 37 °C and 5% CO_2 until confluence. The cells were treated with DAHP (5 mmol/L, 81260, Cayman Chemical) for 0, 1, 2, 3, and 6 hours prior to analyses of total superoxide production, eNOS uncoupling activity, mitochondrial superoxide production, as well as expression of ER stress marker PDI.

In brief, DHE was used to measure superoxide production in DAHP-treated PAECs. PAECs were cultured on glass cover slips until confluence and then serum deprived prior to being treated with DAHP (5 mmol/L) for 0, 1, 2, 3, and 6 hours. Cells were incubated with DHE solution (2 μmol/L) in the dark at 37 °C for 30 minutes to determine total superoxide production. To determine eNOS uncoupling activity, cells were incubated with DHE solution in the presence or absence of L-NAME. To measure changes in mitochondrial superoxide production, PAECs treated with DAHP were also incubated with MitoSOX solution (5 μmol/L) for 15 minutes at 37 °C in the dark. A laser scanning confocal microscope (Nikon A1R) was used for acquisition of all fluorescent images. The average fluorescent intensities (normalized by cell numbers) were analyzed and quantified using ImageJ software.

WESTERN BLOT ANALYSIS. Activation of ER stress in DAHP-stimulated PAECs was assessed by examining expression of PDI, an ER stress marker. Cells were lysed in lysis buffer (0.2 mol/L Tris, 1.5 mol/L NaCl, 10 mmol/L EDTA, 10 mmol/L ethylene glycol-bis(/β-aminoethyl ether)-N,N,N',N'-tetra-acetic acid, 25 mmol/L sodium pyrophosphate, 10 mmol/L β-glycerophosphate, 10 mmol/L Na_3VO_4, 1 mmol/L phenylmethanesulfonyl fluoride, 2 μmol/L leupeptin, and 10% Triton, pH 7.4) for 15 minutes on ice, and then centrifuged at 12,000*g* for 10 minutes at 4 °C. The supernatants were transferred to a new Eppendorf tube and protein concentrations were determined using a BCA protein assay kit (#7780, Cell Signaling Technology). Twenty micrograms of cellular proteins were separated in 10% sodium dodecyl sulfate-polyacrylamide gel electrophoresis and transferred to nitrocellulose membranes. The membranes were blocked with 5% nonfat milk at room temperature for 1 hour, and then incubated with antibody for PDI (1:1000, ab2792, Abcam) at 4 °C overnight. After washing with PBST and subsequent incubation with goat anti-mouse secondary antibody (1:1000), the membranes were washed again with PBST and the expression levels of PDI were assessed by chemiluminescent detection with ECL reagent (WBKLS0100, MilliporeSigma). The intensity of the target bands was analyzed and quantified using ImageJ software.

MITOCHONDRIAL ISOLATION AND SWELLING ASSAY. Freshly isolated lung tissues were rinsed twice in ice-cold Krebs/HEPES buffer, and homogenized in a prechilled glass homogenizer using isolation buffer I (sucrose 250 mmol/L, ethylene glycol-bis(/β-aminoethyl ether)-N,N,N',N'-tetra-acetic acid 1 mmol/L, 4-(2-hydroxyethyl)piperazine-1-ethanesulfonic acid 10 mmol/L, and Tris-HCl 10 mmol/L, pH 7.4, 1 mL buffer/0.33 g tissue) on ice. The homogenates were then centrifuged at 800*g* for 7 minutes at 4 °C, followed by additional centrifugation at 4,000*g* for 15 minutes at 4 °C. The pellet was resuspended using 1 mL of isolation buffer II (isolation buffer I without ethylene glycol-bis(/β-aminoethyl ether)-N,N,N',N'-tetra-acetic acid), and then centrifuged again at 4,000*g* for 15 minutes at 4 °C. Further purification

was performed as previously described.[33] Then, the pellet was resuspended with 100 μL of isolation buffer II.

For mitochondrial swelling assay to examine integrity of the mitochondria, 100 μg of freshly isolated mitochondria were mixed in swelling buffer (sucrose 250 mmol/L, Tris-HCl 10 mmol/L, pH 7.4). The mixture was then incubated with 5 mmol/L succinate for 1 minute at room temperature, then with 250 μmol/L of $CaCl_2$. Absorbance at 540 nm was measured immediately for 20 minutes at 1-minute intervals using a BioTek Plate Reader (BioTek). Swelling was measured as a decrease in absorbance over time.

TRANSMISSION EM ANALYSIS OF MITOCHONDRIAL STRUCTURAL CHANGES. Transmission EM was used to assess mitochondrial morphology in freshly isolated lung tissues. Lung tissues were finely diced (2-mm cubes) and collected into 2.5% glutaraldehyde for 1-2 hours at room temperature. Strips were washed in 0.1 mol/L phosphate buffer solution (PBS, pH 7.4) for 3 changes of 10 minutes each. Samples were postfixed in 1% osmium tetroxide in PBS for 1 hour on ice, washed twice, transferred to 2% aqueous uranyl acetate for 20 minutes, and then dehydrated through successive washes in 30%, 50%, 70%, 95%, and absolute acetone. The samples were incubated overnight in acetone/resin (50:50). After a final incubation in resin overnight, samples were embedded in fresh resin polymerized at 60 °C for 48 hours. The samples were sectioned (100 nm) using an ultramicrotome (Ultra Cut UCT, Leica Microsystems), placed on grids, and allowed to dry overnight. The samples on grids were then stained using 2% uranyl acetate in ultrapure water and Reynolds lead citrate. Grids were examined using a transmission EM (JEM-1400 PLUS, JEOL) at 80 kV and images captured using a digital camera.

IN VIVO TREATMENT WITH MitoTempo TO SCAVENGE MITOCHONDRIAL ROS. Mice were randomly divided into 5 groups: a normal control group (n = 4); a DAHP group (n = 7); a DAHP group treated with MitoTempo (DAHP + MitoTempo, n = 5); a hypoxia group (n = 7); and a hypoxia group treated with MitoTempo (Hypoxia + MitoTempo, n = 5). MitoTempo was dissolved in PBS and used to treat mice by daily intraperitoneal injection (0.7 mg/kg/d, ALX-430-150, Enzo Life Sciences International Inc) starting 2 days prior to DAHP/hypoxia treatment and throughout the entire treatment protocol of DAHP (10 mmol/L)/hypoxia (10% oxygen) for 3 weeks. After 3 weeks, hemodynamic parameters of mPAP and RVSP, histologic features of vascular remodeling, eNOS uncoupling activity, mitochondrial superoxide production, as well as intracellular NO levels were determined as described.

STATISTICAL ANALYSIS. All data are presented as mean ± SEM. Statistical analyses were performed using GraphPad Prism (version 9.5.1, Dotmatics). Normality was assessed using the Shapiro-Wilk test. Differences were considered statistically significant if $P < 0.05$ by Student's *t*-test for comparison between 2 groups, or by 1-way analysis of variance for multigroup comparison that was followed by Dunnet or Newman-Keuls multiple comparison test.

RESULTS

RECOUPLING OF eNOS OR ATTENUATION OF ER STRESS PREVENTED PH IN BOTH DAHP AND HYPOXIA MODELS: HEMODYNAMIC RESPONSES. To examine roles of eNOS uncoupling and ER stress in mediating PH development, and the interrelationship between the 2, mice were induced of PH by DAHP administration or exposure to hypoxia, and treated with FA, PBA, or FA + PBA to attenuate eNOS uncoupling and ER stress in vivo. Hypoxia is a classical model of PH in mice. In addition, we have established a novel murine model of PH by directly inducing eNOS uncoupling and endothelial dysfunction with administration of DAHP to inhibit eNOS cofactor tetrahydrobiopterin synthetic enzyme GCH1. As shown in **Figure 1A**, DAHP administration (10 mmol/L, 3 weeks) markedly elevated mPAP in mice (36.45 ± 3.86 mm Hg, n = 7 for DAHP vs 18.95 ± 0.96 mm Hg, n = 6 for control mice). Recoupling of eNOS with FA diet[37,41-43] reduced mPAP in FA group to baseline (22.39 ± 2.40 mm Hg, n = 5), whereas preservation of ER function with PBA also abolished the increase in mPAP in DAHP-treated animals (to 20.48 ± 1.90 mm Hg, n = 5). Combinatory therapy of FA + PBA did not show additive effects on mPAP in DAHP-treated animals (19.47 ± 2.05 mm Hg, n = 4), indicating that uncoupled eNOS and ER stress align in the same pathway to induce PH (**Figure 1A**). The RVSP data are presented in **Figure 1B** in which DAHP administration induced elevated RVSP (40.83 ± 0.97 mm Hg, n = 7 for DAHP vs 26.79 ± 2.75 mm Hg, n = 6 for control mice). The RVSP was substantially attenuated in the DAHP + FA group (34.23 ± 2.06 mm Hg, n = 5), DAHP + PBA group (32.28 ± 2.77 mm Hg, n = 5), and DAHP + FA + PBA group (32.27 ± 2.18 mm Hg, n = 5).

Similarly, exposure to hypoxia markedly elevated mPAP in mice (40.54 ± 4.47 mm Hg, n = 6) compared to the control group (18.95 ± 0.96 mm Hg, n = 6) (**Figure 1C**). This response was significantly attenuated by treatment with FA, PBA, or FA + PBA to 26.34

FIGURE 1 FA, PBA, and Combination Therapy Significantly Attenuated mPAP) and RVSP Elevated by DAHP Administration or Hypoxia Exposure

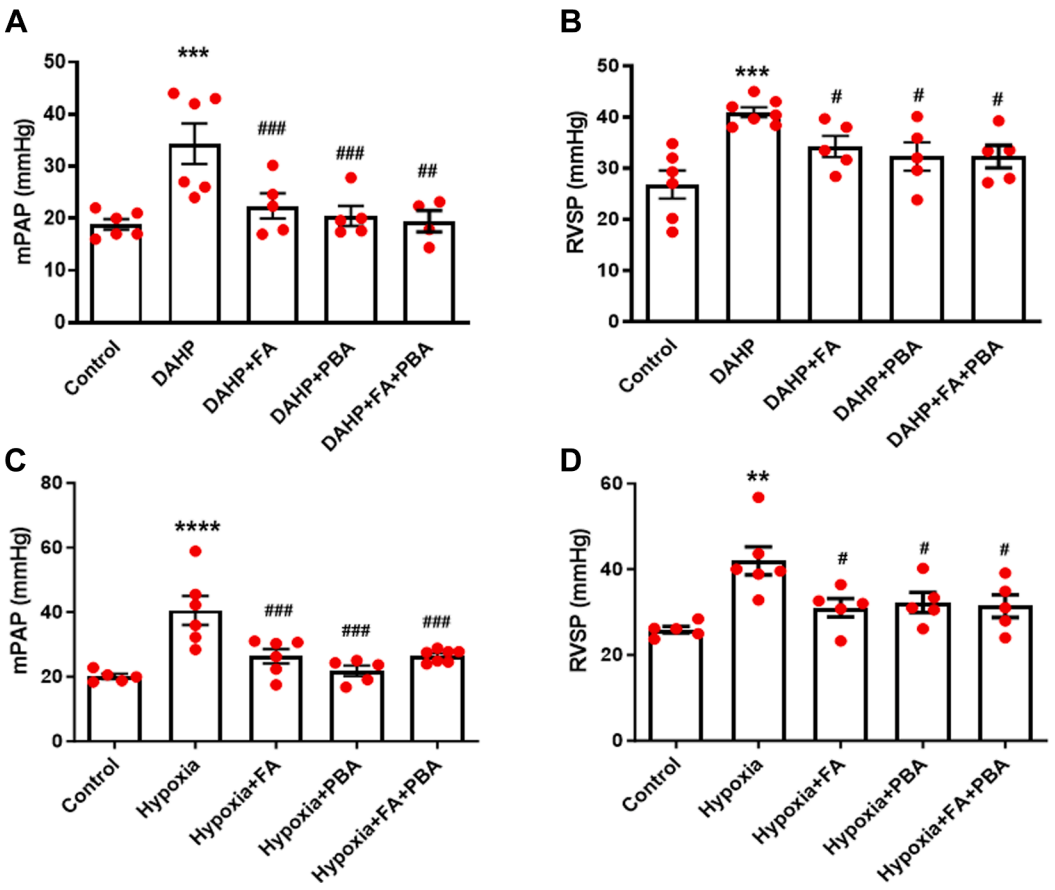

Pulmonary hypertension was induced by 2,4-diamino 6-hydroxypyrimidine (DAHP; 10 mmol/L in drinking water) or hypoxia (normobaric 10% O_2 and 5% CO_2 balanced with 90% N_2) for 3 weeks, and some animals were treated with folic acid (FA), phenylbutyric acid (PBA), or FA + PBA. Control group was given standard mouse chow and regular water. FA, PBA, or FA + PBA was administrated by FA (15 mg/kg/d) chow or PBA (1 g/kg/d) chow or FA + PBA combined chow for both DAHP and hypoxia experiments. Mean pulmonary arterial pressure (mPAP) and right ventricular systolic pressure (RVSP) were recorded by inserting 1.4-F catheter by open chest method using Power Lab data acquisition system. Changes are shown for mPAP in the DAHP model (A), RVSP in DAHP model (B), mPAP in the hypoxia model (C), and RVSP in the hypoxia model (D). All data are expressed as mean ± SEM. n = 4-8. Data were analyzed by 1-way analysis of variance for multigroup comparison that was followed by Dunnet or Newman-Keuls multiple comparison test. $^{**}P < 0.01$ vs control group; $^{***}P < 0.001$ vs control group; $^{****}P < 0.0001$ vs control group; $\#P < 0.05$ vs DAHP or hypoxia groups; $\#\#P < 0.01$ vs DAHP groups; $\#\#\#P < 0.001$ vs DAHP or hypoxia groups.

± 2.24 mm Hg, n = 6; 21.78 ± 1.63 mm Hg, n = 5; and 26.47 ± 0.73 mm Hg, n = 7, respectively. In addition, hypoxia exposure elevated RVSP (41.94 ± 3.287 mm Hg, n = 6) in mice compared to the control mice (26.79 ± 2.75 mm Hg, n = 6), which was also attenuated significantly to baseline by treatment of FA, PBA, or FA + PBA in hypoxia + FA (31.03 ± 2.15 mm Hg, n = 5), hypoxia + PBA (32.25 ± 2.31 mm Hg, n = 5) and hypoxia + FA + PBA (31.41 ± 2.62 mm Hg, n = 5) groups (Figure 1D). These data strongly indicate an intermediate role of aligned signaling pathway of uncoupled eNOS and ER stress in the development of PH.

RECOUPLING OF eNOS OR ATTENUATION OF ER STRESS PREVENTED PULMONARY VASCULAR REMODELING IN BOTH DAHP AND HYPOXIA MODELS OF PH. In PH, vascular remodeling is characterized by increased medial thickness, collagen deposition, and intimal narrowing in small pulmonary arteries.[44,45] We have observed clear medial thickening and collagen deposition in the DAHP and hypoxia

models of PH. As shown in Figures 2A and 2B, DAHP treatment induced a significant increase in the medial wall thickness of all vessels <200 μm in outer diameter as compared to the control group (58.44 ± 3.99, n = 7 vs 25.91 ± 2.96, n = 5). In comparison, treatment with FA, PBA, or FA + PBA completely attenuated this vascular remodeling phenotype of medial wall thickness in DAHP + FA (28.49 ± 2.28, n = 6), DAHP + PBA (33.02 ± 1.28, n = 6), and DAHP + FA + PBA (25.30 ± 0.59, n = 6) groups. Likewise, hypoxia treatment induced a significant increase in the medial wall thickness of all vessels <200 μm in outer diameter as compared to the control group (44.02 ± 2.92, n = 7 vs 25.91 ± 2.96, n = 5) (Figures 2A and 2C). Treatment with FA, PBA, or FA + PBA also markedly attenuated medial thickening in hypoxia + FA (32.48 ± 1.44, n = 6), hypoxia + PBA (28.19 ± 1.73, n = 5), and hypoxia + FA + PBA (29.16 ± 1.58, n = 6) groups, respectively. In all mice, the magnitude of remodeling seemed to increase as vessel diameter decreased, with the greatest degree of vascular remodeling occurring in those vessels with a diameter size between 50 and 200 μm. The magnitude of hypoxic pulmonary vascular remodeling for all vessel sizes was slightly lesser compared to DAHP-treated mice (Figures 2B and 2C).

To gain more insights into the effects on pulmonary vascular remodeling of FA and PBA, we examined expression of smooth muscle α-actin (SMA) in the lung tissue sections using immunohistochemistry. As is obvious in Figures 2D and 2E, we observed markedly increased expression of SMA in the small arteries of mice exposed to DAHP or hypoxia, which was completely attenuated by FA, PBA, or FA + PBA treatment. We further assessed expression levels of the cell proliferation marker proliferating cell nuclear antigen (PCNA). Similarly, the marked increase in PCNA expression in the lung sections of the DAHP- or hypoxia-treated mice was abolished by FA, PBA, or FA + PBA treatment (Figures 2F and 2G). These data further indicate attenuation of vascular remodeling by recoupling of eNOS and alleviation of ER stress in both DAHP and hypoxia models of PH.

RECOUPLING OF eNOS WITH FA OR PRESERVATION OF ER FUNCTION WITH PBA ABROGATED EXPRESSION OF ER STRESS MARKER PDI IN BOTH DAHP AND HYPOXIC MODELS OF PH. To determine whether ER stress is involved in the pathogenesis of PH downstream of uncoupled eNOS, we examined expression levels of the ER stress marker PDI in both DAHP- and hypoxia-induced PH mice. The immunostaining of PDI revealed substantially increased expression of PDI in the pulmonary vascular endothelial cells of mice exposed to DAHP compared to the control group (1,536 ± 168.6, n = 6 vs 356.7 ± 67.18, n = 5) (Figures 3A and 3B). The results demonstrate that ER stress had been induced following exposure to DAHP, which was significantly attenuated by FA (700.5 ± 193.2, n = 6) or PBA treatment (291.5 ± 84.14, n = 5) (Figure 3B). Likewise, data indicate that PDI expression was significantly increased in the pulmonary vascular endothelial cells of mice exposed to hypoxia compared to control mice (2,069 ± 234.6, n = 6 vs 606.4 ± 97.47, n = 11) (Figures 3A and 3C), and this response was substantially attenuated by FA (750.3 ± 170.1, n = 7) or PBA (331.8 ± 51.74, n = 9). These data indicate that eNOS uncoupling lies upstream of ER stress during pathogenesis of PH. Combinatory treatment with FA and PBA had no additional effects, indicating eNOS uncoupling is upstream of ER stress in the same signaling axis.

eNOS UNCOUPLING AND FEED-FORWARD REGULATION OF ER STRESS AND MITOCHONDRIAL DYSFUNCTION ON eNOS UNCOUPLING IN DAHP AND HYPOXIA MODELS OF PH. Total superoxide production and eNOS uncoupling activity were assessed with dihydroethidium (DHE) fluorescent imaging in the presence or absence of L-NAME in the lung sections of both DAHP- and hypoxia-treated mice (Figures 4A to 4C). DHE fluorescent intensity was significantly increased in mice exposed to 3 weeks of DAHP (12.61 ± 1.27, n = 23 vs 27.51 ± 3.96, n = 23 for control vs DAHP groups). Treatment with FA, PBA, or FA + PBA substantially attenuated superoxide signal detected by DHE (from 27.51 ± 3.96, n = 23 in the DAHP group to 16.52 ± 2.058, n = 20, 16.08 ± 2.412, n = 21, and 11.79 ± 2.17, n = 21 for DAHP + FA, DAHP + PBA, and DAHP + FA + PBA groups, respectively). Addition of L-NAME resulted in increased fluorescent intensity in the control group (12.61 ± 1.271, n = 23 vs 15.06 ± 2.392, n = 18 for control vs control + L-NAME groups), indicating loss of NO from coupled eNOS resulted in more measured superoxide. Addition of L-NAME resulted in decreased fluorescent intensity in the DAHP experimental group (16.30 ± 2.75, n = 16 vs 27.51 ± 3.96, n = 23 for DAHP + L-NAME vs DAHP groups), indicating uncoupling of eNOS. As expected, FA treatment recoupled eNOS to eliminate L-NAME-dependent superoxide production, whereas PBA treatment also attenuated eNOS uncoupling activity, indicating benefits of ER stress correction via shutting down of the ER stress-eNOS uncoupling feed-forward mechanism. The combinatory therapy with FA and PBA displayed similar effects on recoupling of eNOS as shown in Figures 4A and 4B.

FIGURE 2 **FA, PBA, and Combination Therapy Attenuated Lung Vascular Remodeling in Both DAHP- and Hypoxia-induced PH Mice**

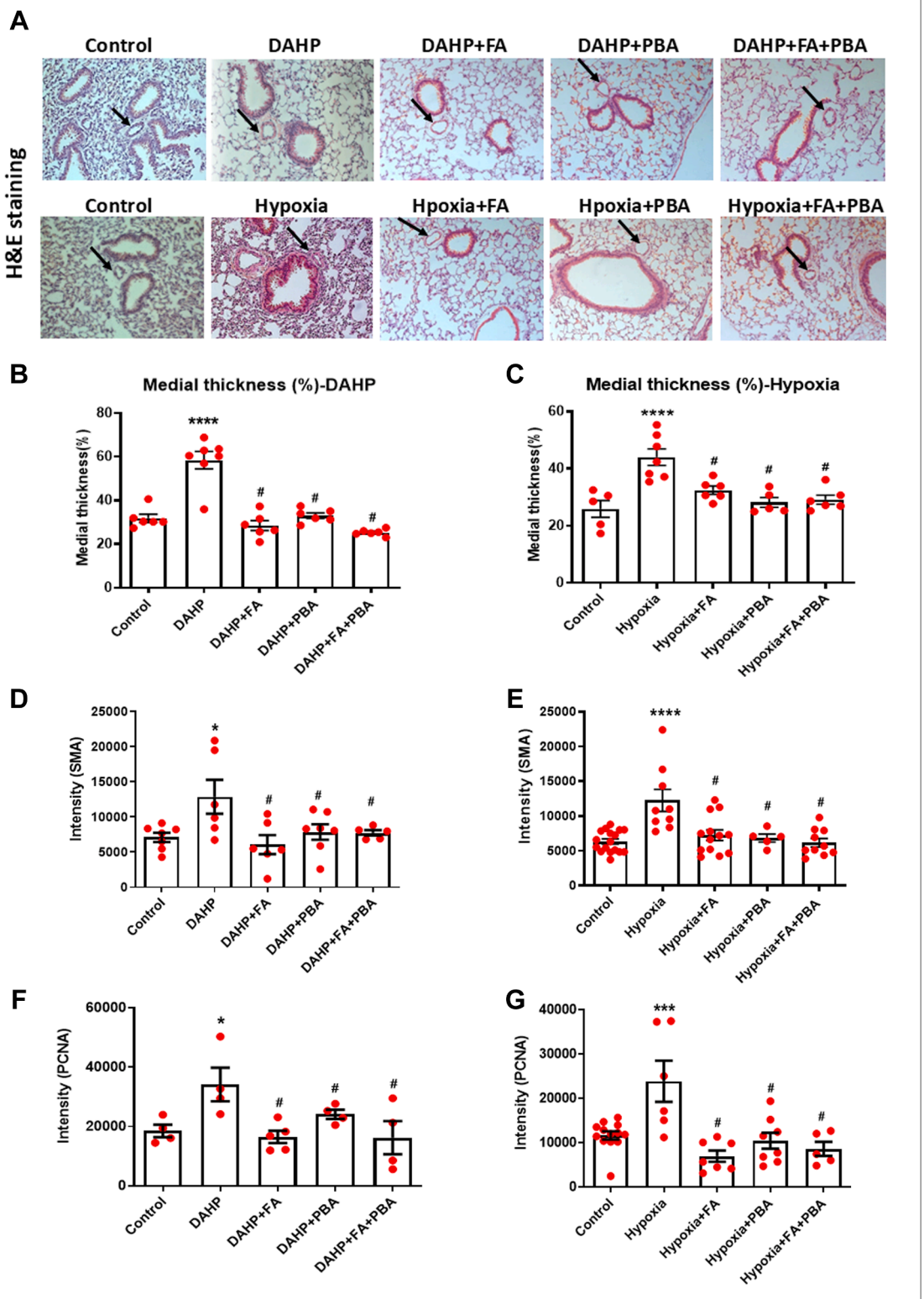

Continued on the next page

As shown in Figures 4A and 4C, DHE intensity was significantly elevated in mice exposed to chronic hypoxia for 3 weeks (9.37 ± 0.59, n = 32 vs 22.11 ± 2.84, n = 28 for control vs hypoxia groups). Treatment with FA, PBA, or FA + PBA substantially attenuated superoxide signal detected by DHE (from 22.11 ± 2.84, n = 28 in the hypoxia group to 13.10 ± 1.18, n = 33, 12.59 ± 1.04, n = 34, 13.10 ± 1.13, n = 29 for hypoxia + FA, hypoxia + PBA, hypoxia + FA + PBA groups, respectively). Addition of L-NAME resulted in increased fluorescent intensity in the control group (9.37 ± 0.59, n = 32 vs 10.06 ± 0.77, n = 22 for control vs control + L-NAME groups), indicating that eNOS is healthy and coupled. Addition of L-NAME resulted in decreased fluorescent intensity in the hypoxia group (11.55 ± 1.89, n = 31 vs 22.11 ± 2.84, n = 28 for hypoxia + L-NAME vs hypoxia groups), indicating uncoupling of eNOS. Of note, FA treatment recoupled eNOS, whereas PBA treatment also attenuated eNOS uncoupling activity, indicating benefits of ER stress correction via shutting down of the ER stress-eNOS uncoupling feed-forward mechanism. Combinatory therapy with FA and PBA also recoupled eNOS consistently.

As shown in Figure 4D, superoxide levels detected by ESR were significantly increased in mice exposed to 3 weeks of DAHP (11.87 ± 1.31 μmol/L/min/mg protein, n = 5 vs 16.94 ± 2.92 μmol/L/min/mg protein, n = 7 for control vs DAHP groups). Furthermore, ESR data indicate that superoxide production was markedly attenuated to baseline in animals subjected to FA treatment (9.67 ± 0.63 μmol/L/min/mg protein, n = 6 for DAHP + FA), PBA treatment (6.77 ± 3.32 μmol/L/min/mg protein, n = 4 for DAHP + PBA), or combination therapy (12.72 ± 2.50 μmol/L/min/mg protein, n = 6 for DAHP + FA + PBA).

Addition of L-NAME resulted in decreased superoxide production in the DAHP group (16.94 ± 2.92 μmol/L/min/mg protein, n = 7 vs 6.32 ± 1.63 μmol/L/min/mg protein, n = 7 DAHP vs DAHP + L-NAME), indicating eNOS-derived superoxide production/uncoupling of eNOS. Addition of L-NAME resulted in increased superoxide production in FA group, PBA group, and the combination therapy group, indicating recoupling of eNOS (Figure 4D).

Likewise in the hypoxia-induced PH model, superoxide levels detected by ESR were significantly increased in mice exposed to 3 weeks of hypoxia (11.87 ± 1.31 μmol/L/min/mg protein, n = 5 vs 31.67 ± 3.17 μmol/L/min/mg protein, n = 5 for control vs hypoxia groups). Superoxide production was markedly attenuated to baseline by FA treatment (10.17 ± 1.70 μmol/L/min/mg protein, n = 5 vs for hypoxia + FA), PBA treatment (11.20 ± 1.96 μmol/L/min/mg protein, n = 5 for hypoxia + PBA), or combination therapy (10.03 ± 1.68 μmol/L/min/mg protein, n = 6 for hypoxia + FA + PBA) (Figure 4E).

Addition of L-NAME resulted in decreased superoxide production in the hypoxia group (31.67 ± 3.17 μmol/L/min/mg protein, n = 5 vs 15.01 ± 2.68, n = 5 for hypoxia vs hypoxia + L-NAME), indicating uncoupling of eNOS. Of note, FA treatment recoupled eNOS, whereas PBA treatment also attenuated eNOS uncoupling activity, indicating benefits of ER stress correction via shutting down of the ER stress-eNOS uncoupling feed-forward mechanism. Combinatory therapy with FA and PBA also recoupled eNOS consistently (Figure 4E).

RECOUPLING OF eNOS OR ATTENUATION OF ER STRESS PRESERVES NO BIOAVAILABILITY IN BOTH DAHP AND HYPOXIC MODELS OF PH. NO levels in lung sections were assessed by measuring DAF-FM DA fluorescent intensity. As shown in Figures 5A and 5B, DAHP administration (10 mmol/L, 3 weeks) markedly reduced NO bioavailability in lung tissues of DAHP-treated mice (25.32 ± 2.78, n = 7 vs 53.82 ± 5.38, n = 5 for DAHP vs control groups). Recoupling of eNOS with FA restored NO levels in DAHP + FA group to baseline (52.15 ± 4.71, n = 5 vs 25.45 ± 3.99, n = 5 for DAHP + FA vs DAHP), whereas preservation

FIGURE 2 Continued

Lung tissues were harvested after pressure measurement, fixed in paraformaldehyde, sectioned, and stained for hematoxylin and eosin (H&E). In additional experiments smooth muscle α-actin (SMA) and proliferating cell nuclear antigen (PCNA) expression was determined by immunohistochemistry. (A-C) Representative images and grouped data for medial thickness indicating that FA, PBA, and combination therapy attenuate medial hypertrophy in arteries <200 μm in outer diameter size in both DAHP- and hypoxia-induced pulmonary hypertensive (PH) mice. (D,E) Fluorescent intensities of SMA expression in DAHP- and hypoxia-induced PH mice. (F,G) Fluorescent intensities of PCNA expression in DAHP- and hypoxia-induced PH mice. Black arrows point to pulmonary blood vessels. All data are expressed as mean ± SEM, n = 5-6 each. Data were analyzed by 1-way analysis of variance for multigroup comparison that was followed by Dunnet multiple comparison test. *$P < 0.05$ vs control group; ***$P < 0.001$ vs control group; ****$P < 0.0001$ vs control group; #$P < 0.05$ vs DAHP or hypoxia groups. Abbreviations as in Figure 1.

FIGURE 3 **FA, PBA, and Combination Therapy Abrogated Expression of ER Stress Marker PDI in Both DAHP- and Hypoxia-induced PH Mice**

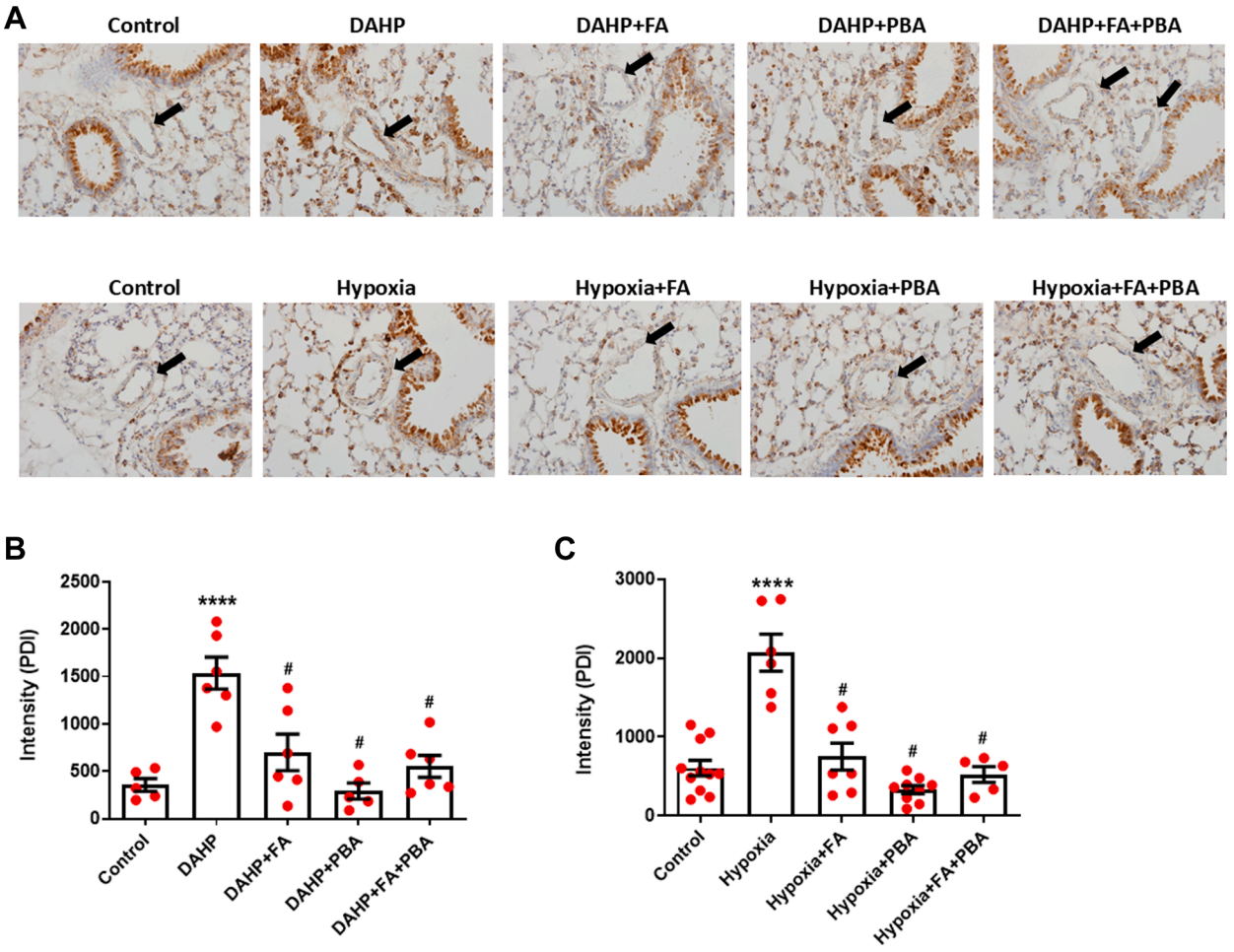

Lung tissues were harvested after pressure measurement, fixed in paraformaldehyde, sectioned, and stained for protein disulfide isomerase (PDI). (A) Representative immunohistochemical images of PDI staining in DAHP and hypoxia animals treated with FA, PBA, or FA + PBA. (B,C) Grouped quantitative data of PDI expression in DAHP and hypoxia animals with different treatments. Data indicate that FA, PBA, or FA + PBA completely abrogated expression of ER stress marker PDI. Black arrows point to pulmonary blood vessels. All data are expressed as mean ± SEM, n = 5-7. Data were analyzed by 1-way analysis of variance for multigroup comparison that was followed by Dunnet multiple comparison test. ***$P < 0.001$ vs control group; *****$P < 0.0001$ vs control group; #$P < 0.01$ vs DAHP or hypoxia groups. ER = endoplasmic reticulum; other abbreviations as in Figures 1 and 2.

of ER function with PBA also markedly recovered NO bioavailability in DAHP + PBA group (48.72 ± 4.28, n = 5 vs 25.45 ± 3.99, n = 5 for DAHP + PBA vs DAHP). This goes along with the notion earlier that ER stress further facilitates eNOS uncoupling via feed-forward mechanism and that correction of ER stress recoupled eNOS. Furthermore, combinatory therapy of FA + PBA had similar effects in improving NO bioavailability in DAHP-treated animals (51.62 ± 4.92, n = 5 vs 25.45 ± 3.99, n = 5 for DAHP + FA + PBA vs DAHP). Likewise, data presented in Figures 5A and 5C indicate that in the hypoxia-induced PH group, NO levels were significantly reduced in mice exposed to hypoxia (33.06 ± 3.45, n = 7 vs 53.82 ± 5.38, n = 5 for hypoxia vs control groups), which, however, was attenuated in hypoxia + FA (51.64 ± 4.18, n = 5 vs 53.82 ± 5.38, n = 5 for hypoxia + PBA vs hypoxia), hypoxia + PBA (49.27 ± 4.06, n = 5 vs 53.82 ± 5.38, n = 5 for hypoxia + PBA vs hypoxia), and hypoxia + FA + PBA (47.41 ± 1.51, n = 5 vs 53.82 ± 5.38, n = 5 for hypoxia + FA + PBA vs hypoxia) groups. We believe the preserved NO bioavailability downstream of

FIGURE 4 FA, PBA, and Combination Therapy Attenuated Lung Vascular ROS Production and eNOS Uncoupling Activity in Both DAHP- and Hypoxia-induced PH Mice

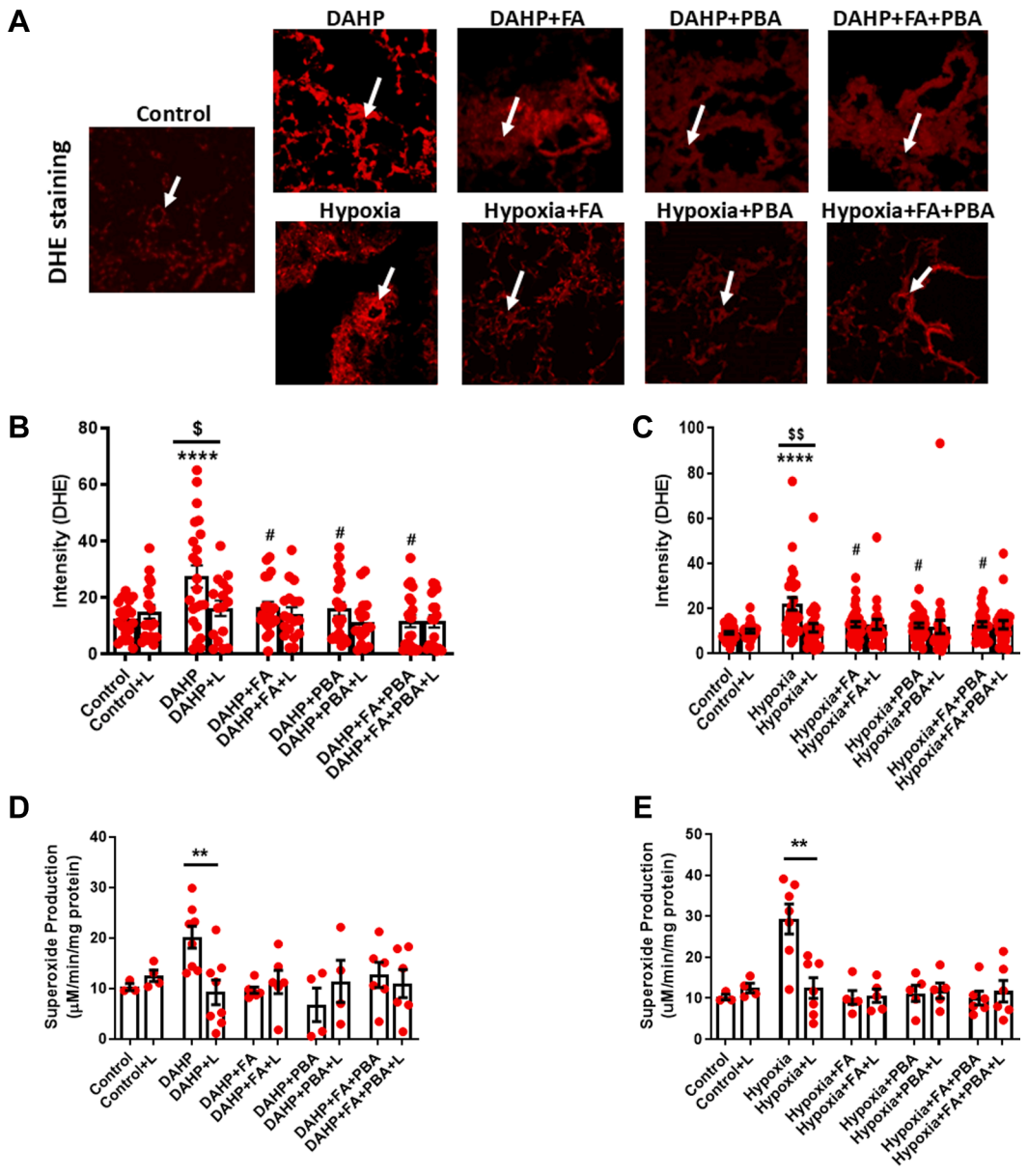

Freshly harvested lung tissues were embedded in optimal cutting temperature compound, sectioned and stained immediately with dihydroethidium (DHE) in the presence or absence of nitric oxide synthase (NOS) inhibitor L-NG-nitro arginine methyl ester, L-NAME (L). (A) Representative DHE images indicating total superoxide production in DAHP and hypoxia groups with different treatments of FA, PBA, or FA + PBA. (B,C) Grouped data of superoxide production (fluorescent intensity) in DAHP and hypoxia animals treated with FA, PBA, or FA + PBA. In normal conditions, L-NAME increases measured superoxide by reducing NO's scavenging effects on superoxide. When endothelial nitric oxide synthase (eNOS) is uncoupled, L-NAME decreases eNOS-derived superoxide production. This is the same for DHE experiments and electron spin resonance analyses (D,E). Data indicate that FA, PBA, or combination therapy attenuated lung vascular reactive oxygen species (ROS) production and eNOS uncoupling activity. White arrows point to pulmonary blood vessels. All data are expressed as mean ± SEM, n = 16-34. Data were analyzed by 1-way analysis of variance for multigroup comparison that was followed by Dunnet multiple comparison test. $^{**}P < 0.01$ vs control group; $^{***}P < 0.001$ vs control group; $^{****}P < 0.0001$; #$P < 0.05$ vs DAHP or hypoxia groups. Abbreviations as in Figures 1 and 2.

FIGURE 5 **FA, PBA, and Combination Therapy Improved NO Bioavailability in Both DAHP, and Hypoxia-induced PH Mice**

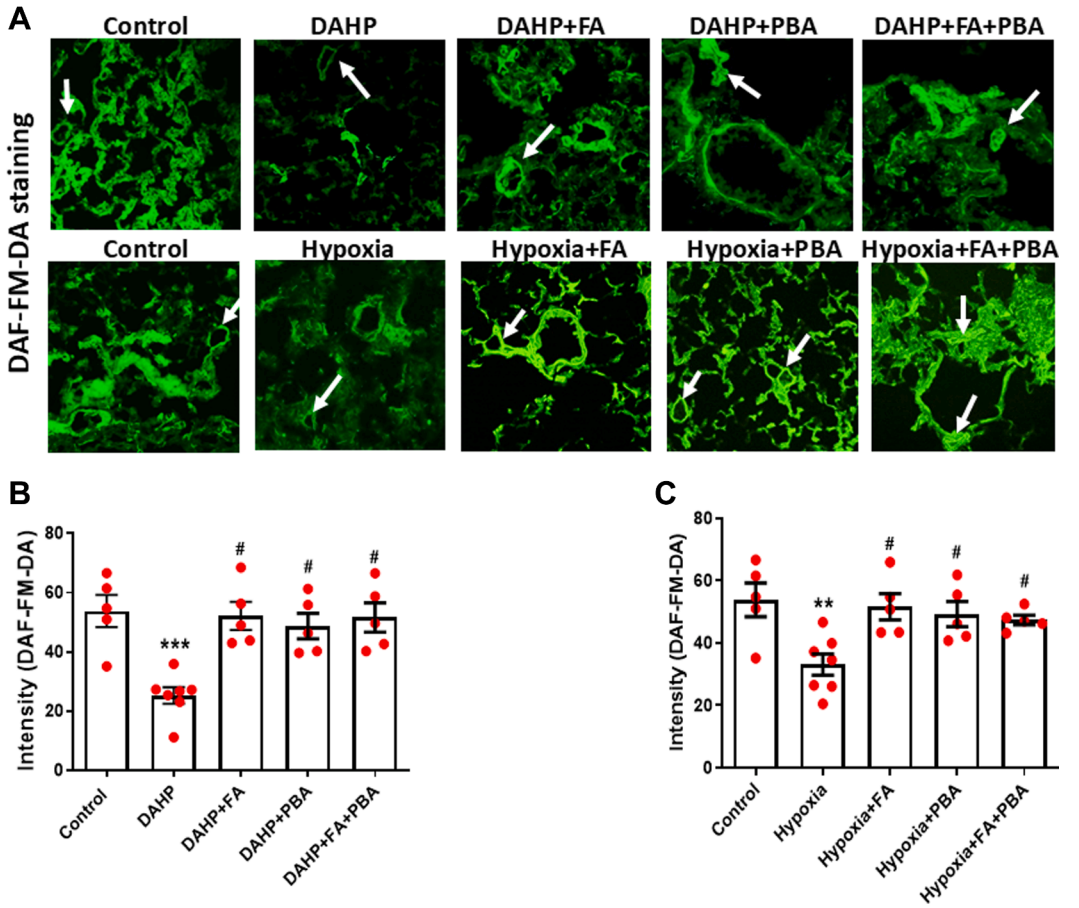

Freshly harvested lung tissues were embedded in optimal cutting temperature compound, sectioned, and stained immediately with 4-amino-5-methylamino-2′,7′-difluorofluorescein diacetate (DAF-FM DA), which is a specific fluorescent probe for intracellular NO. (A-C) Shown are the representative fluorescent images from each group and the grouped data of NO bioavailability (fluorescent intensity) in DAHP and hypoxia animals treated with FA, PBA, or FA + PBA. Data indicate that FA, PBA, or FA + PBA completely restored NO bioavailability in pulmonary vasculature of PH mice. White arrows point to pulmonary blood vessels. All data are expressed as mean ± SEM, n = 5 each. Data were analyzed by 1-way analysis of variance for multigroup comparison that was followed by Dunnet multiple comparison test. *P < 0.05 vs control group; **P < 0.01 vs control group; #P < 0.05 vs DAHP or hypoxia groups. Abbreviations as in Figures 1 and 2.

restoration of eNOS coupling activity represents a major intermediate pathway in attenuating PH phenotypes in FA- and PBA-treated PH mice.

RECOUPLING OF eNOS WITH FA OR PRESERVATION OF ER FUNCTION WITH PBA PREVENTED MITOCHONDRIAL DYSFUNCTION IN BOTH DAHP AND HYPOXIC AND MODELS OF PH. To assess a role of mitochondrial dysfunction in PH development, we detected mitochondrial ROS production using MitoSOX in freshly isolated lung issues of DAHP- or hypoxia-treated mice. As shown in Figure 6A, lung tissues treated with DAHP had markedly increased mitochondrial ROS production (35.24 ± 4.48 n = 36 vs 18.70 ± 2.95 n = 25 for DAHP vs control groups) as shown by quantified fluorescent intensity of MitoSOX Red. This response was completely attenuated in DAHP + FA (15.49 ± 2.59, n = 8), DAHP + PBA (13.60 ± 2.27, n = 16), and DAHP + FA + PBA (14.49 ± 3.61, n = 17) groups, respectively (Figure 6B). Similarly, MitoSOX fluorescent intensity was markedly elevated in hypoxia-treated animals (30.39 ± 2.83, n = 36 vs 20.50 ± 2.69, n = 32 for hypoxia vs control groups), which was also attenuated to baseline by FA, PBA, or FA + PBA treatment in the hypoxia + FA (19.91 ± 1.31, n = 30), hypoxia + PBA (23.20 ± 2.08, n = 33), and hypoxia + FA + PBA (21.62 ± 1.92, n = 28) groups, respectively (Figure 6C).

FIGURE 6 FA, PBA, and Combination Therapy Attenuated Mitochondrial ROS Production in Both DAHP- and Hypoxia-induced PH Mice

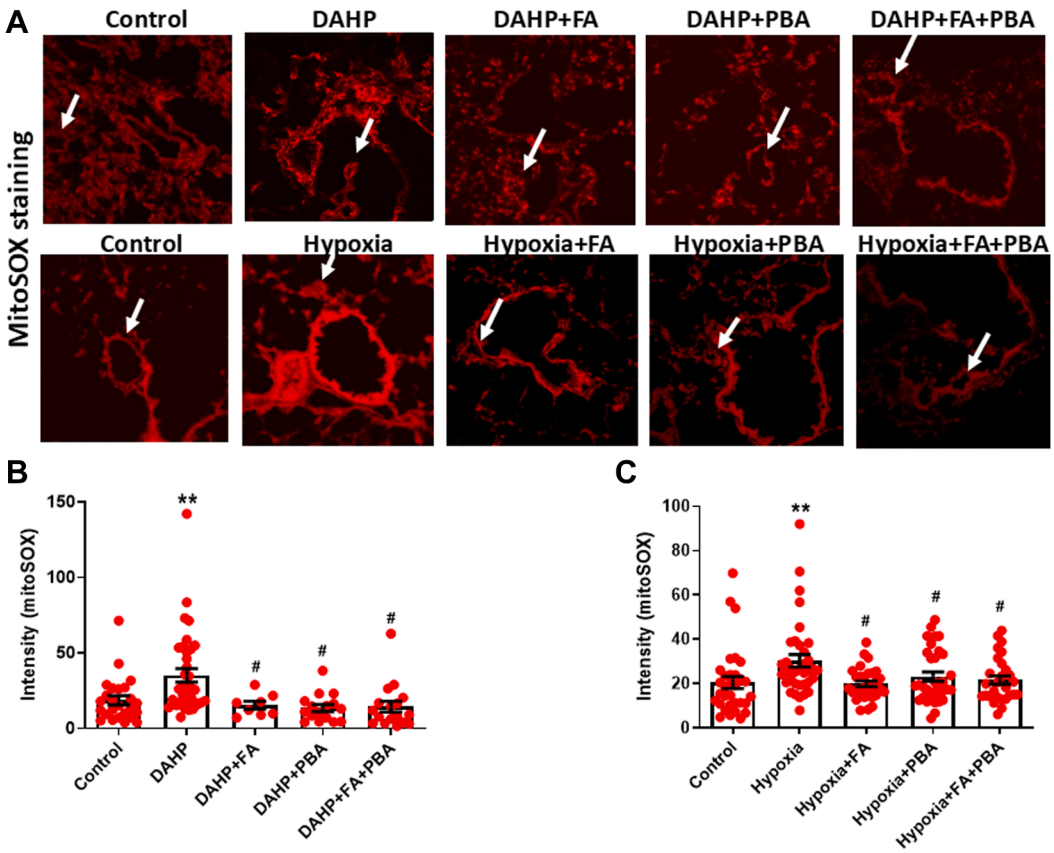

Freshly harvested lung tissues were embedded in optimal cutting temperature compound, sectioned, and stained immediately with MitoSOX Red reagent for detection of mitochondrial ROS production. (A-C) Shown are the representative fluorescent images and grouped data for mitochondrial ROS production in DAHP and hypoxia mice with different treatments. Data indicate FA, PBA, or FA + PBA completely attenuated mitochondrial ROS production in both DAHP and hypoxia mice. White arrows points to pulmonary blood vessels. All data are expressed as mean ± SEM, n = 16-36. Data were analyzed by 1-way analysis of variance for multigroup comparison that was followed by Dunnet multiple comparison test. $^{**}P < 0.01$ vs control group; $^{***}P < 0.001$ vs control group; $\#P < 0.05$ vs DAHP or hypoxia groups. Abbreviations as in Figures 1, 2, and 4.

As shown in Figures 7A and 7B, calcium-induced mitochondrial swelling activity was markedly increased in DAHP- or hypoxia-treated mice, indicating impaired mitochondrial integrity. Treatment with FA to recouple eNOS or PBA to preserve ER function completely attenuated mitochondrial swelling activity. Taken together with the inhibitory effects on mitochondrial ROS production described, these data indicate that uncoupled eNOS and ER stress lie upstream of mitochondrial dysfunction in inducing PH.

Mitochondrial morphology is a critical factor influencing the efficiency of mitochondrial adenosine triphosphate synthesis. Further studies using EM demonstrate that in both DAHP and hypoxic models of PH, there was a robust distortion of cristae structure of mitochondria (Figures 8A and 8B), with the black arrows indicating mitochondria with typical disorganized cristae; and this response was completely alleviated by treatment with FA or PBA in both DAHP- and hypoxia-induced PH models. Combinatory treatment with FA and PBA had no additive effects on mitochondrial cristae structures examined by EM. These data further confirm an eNOS uncoupling/ER stress/mitochondrial dysfunction signaling axis in mediating pathogenesis of PH.

PRESERVATION OF MITOCHONDRIAL FUNCTION WITH MitoTempo ATTENUATED PHENOTYPES OF PH IN BOTH DAHP AND HYPOXIC MODELS. To examine a previously unestablished causal role of mitochondrial dysfunction in PH development,

FIGURE 7 FA, PBA, and Combination Therapy Abrogated Enhanced Mitochondrial Swelling in Both DAHP- and Hypoxia-induced PH Mice

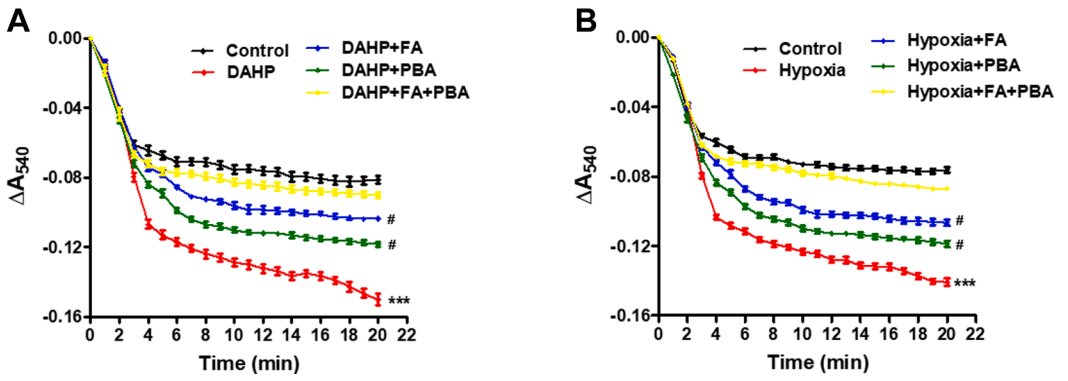

Freshly isolated mitochondria from homogenized lung tissues were mixed in swelling buffer, incubated with 5 mmol/L succinate and then 250 μmol/L of $CaCl_2$, prior to measurement of absorbance at 540 nm. A steeper decline in the absorbance indicates increased swelling of mitochondria and impaired mitochondrial integrity. (A,B) Grouped data of mitochondrial swelling activities in FA-, PBA-, and FA + PBA–treated DAHP and hypoxia animals are shown. All data are expressed as mean ± SEM, n = 5-6. Data were analyzed using 1-wayanalysis of variance for longitudinal data. ***$P < 0.001$ vs control group; #$P < 0.05$ vs DAHP or hypoxia groups.

we investigated effects on PH development of in vivo treatment with MitoTempo, a mitochondrion-targeted ROS scavenger. Mice were treated by daily intraperitoneal injection (0.7 mg/kg/d) of MitoTempo starting 2 days prior to DAHP or hypoxia stimulation and throughout the entire treatment protocol of 3 weeks. Features of hemodynamic changes, pulmonary vascular remodeling, and NO levels were examined after 3 weeks. As shown in **Figure 9A**, DAHP administration (10 mmol/L, 3 weeks) markedly elevated mPAP in mice (36.45 ± 3.86 mm Hg, n = 7 vs 18.95 ± 0.96 mm Hg, n = 6 for DAHP vs control groups). Treatment with MitoTempo substantially reduced mPAP to 26.02 ± 2.31 mm Hg, n = 5. Similarly, hypoxia exposure elevated mPAP in mice (40.54 ± 4.47 mm Hg, n = 6 vs 18.95 ± 0.96 mm Hg, n = 6 for hypoxia vs control groups). Treatment with MitoTempo markedly reduced mPAP to 21.97 ± 1.68 mm Hg, n = 5. The RVSP data are presented in **Figure 9B** in which DAHP administration induced elevated RVSP (40.83 ± 0.97 mm Hg, n = 7 vs 26.79 ± 2.74 mm Hg, n = 6 for DAHP vs control groups). The RVSP was also substantially attenuated in the MitoTempo group (32.95 ± 2.40 mm Hg, n = 5). Likewise, hypoxia exposure markedly elevated RVSP in mice (41.94 ± 3.28 mm Hg, n = 7 vs 26.79 ± 2.74 mm Hg, n = 6 for hypoxia vs control groups). Treatment with MitoTempo substantially reduced RVSP to baseline to 31.48 ± 2.06 mm Hg, n = 5.

Percentage medial thickness in small pulmonary arteries was assessed. As shown in **Figure 9C**, DAHP treatment induced a significant increase in the medial wall thickness of all vessels sized <200 μm as compared to the control group (58.44 ± 3.99, n = 7 vs. 25.91 ± 2.96, n = 5 for DAHP vs control groups). In comparison, treatment with MitoTempo substantially attenuated vascular medial wall thickness (33.43 ± 4.23, n = 5). Likewise, in the hypoxia model, data presented in **Figure 9D** indicate that hypoxia exposure induced a significant increase in the external diameter of all vessels sized <200 μm as compared to the control group (44.02 ± 2.92, n = 7 vs 25.91 ± 2.96, n = 5 for hypoxia vs control groups). In comparison, treatment with MitoTempo completely attenuated this phenotype of vascular medial remodeling (25.90 ± 0.8796, n = 5). These data suggest that DAHP induced slightly stronger vascular remodeling in small sized blood vessels compared to hypoxia, whereas MitoTempo was effective in attenuating medial thickening in PH induced by both DAHP and hypoxia.

Vascular remodeling was determined by SMA immunofluorescent staining. As shown in **Figure 9E**, SMA intensity was significantly increased in DAHP group compared to control (32.36 ± 1.36 vs 17.01 ± 2.12 for DAHP vs control groups). Treatment with MitoTempo substantially attenuated vascular remodeling induced by DAHP (17.25 ± 2.46). Similarly, SMA intensity was significantly increased in hypoxia group compared to control (27.37 ± 1.78 vs 17.01 ± 2.12 for hypoxia vs control groups). Treatment with MitoTempo also substantially attenuated vascular remodeling induced by hypoxia (15.68 ± 2.813).

FIGURE 8 FA, PBA, and Combination Therapy Preserved Mitochondrial Crystae Structures in Both DAHP- and Hypoxia-induced PH Mice

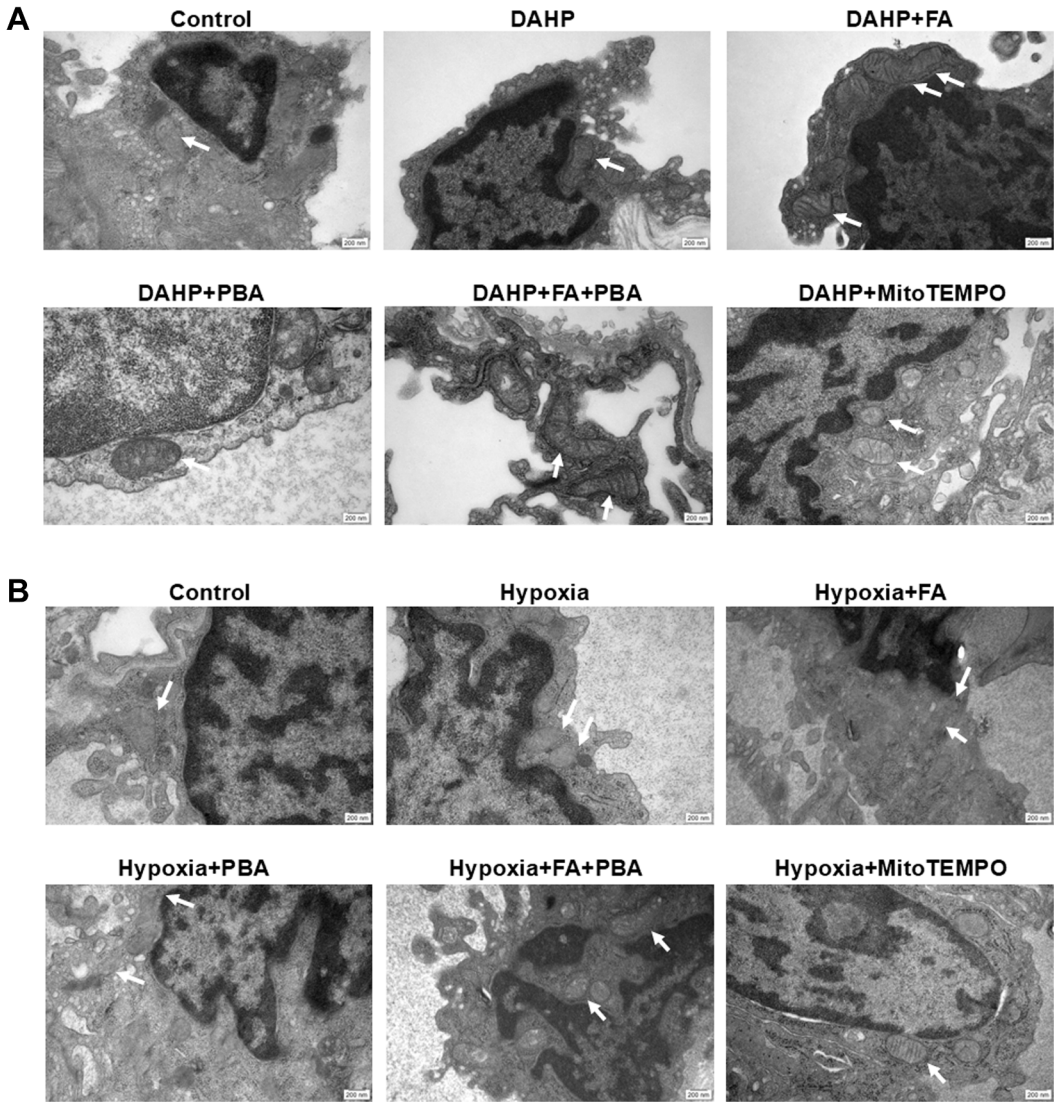

Lung tissues were finely diced (2-mm cubes) and collected into 2.5% glutaraldehyde for 1-2 hours at room temperature. Strips were washed in in 0.1 mol/L phosphate-buffered saline solution (pH 7.4) and then postfixed in 1% osmium tetroxide, transferred to 2% aqueous uranyl acetate for 20 minutes, and dehydrated. The samples were incubated overnight in acetone/resin (50:50). After a final incubation in resin overnight, they were embedded in fresh resin polymerized at 60 °C for 48 hours. The samples were sectioned for thin tissue samples (100 nm), using an ultra-microtome (Ultra Cut UCT). Samples were then stained using 2% uranyl acetate in ultrapure water and Reynolds lead citrate. Grids were examined in a transmission electron microscope. (A,B) Shown are the representative electron microscopy images from each group in DAHP- or hypoxia-induced PH mice. As is obvious, DAHP or hypoxia induced destruction of mitochondrial crystae structures, which, however, were substantially alleviated in FA-, PBA-, and FA + PBA-treated groups. Arrows indicate mitochondria in the pulmonary vascular endothelial cells. Abbreviations as in Figures 1 and 2.

Proliferating cells were determined by PCNA immunofluorescent staining. As shown in Figure 9F, PCNA intensity was significantly increased in DAHP group compared to control (24.30 ± 1.62 vs. 11.97 ± 2.54 for DAHP vs control groups). Treatment with MitoTempo substantially attenuated vascular remodeling induced by DAHP (16.88 ± 1.313). Similarly, SMA intensity was significantly increased in hypoxia group compared to control (21.22 ± 2.06 vs 11.97 ± 2.54 for hypoxia vs control group). Treatment

FIGURE 9 In vivo MitoTempo Treatment Attenuated mPAP/RVSP and Vascular Remodeling in Both DAHP- and Hypoxia-induced PH Mice

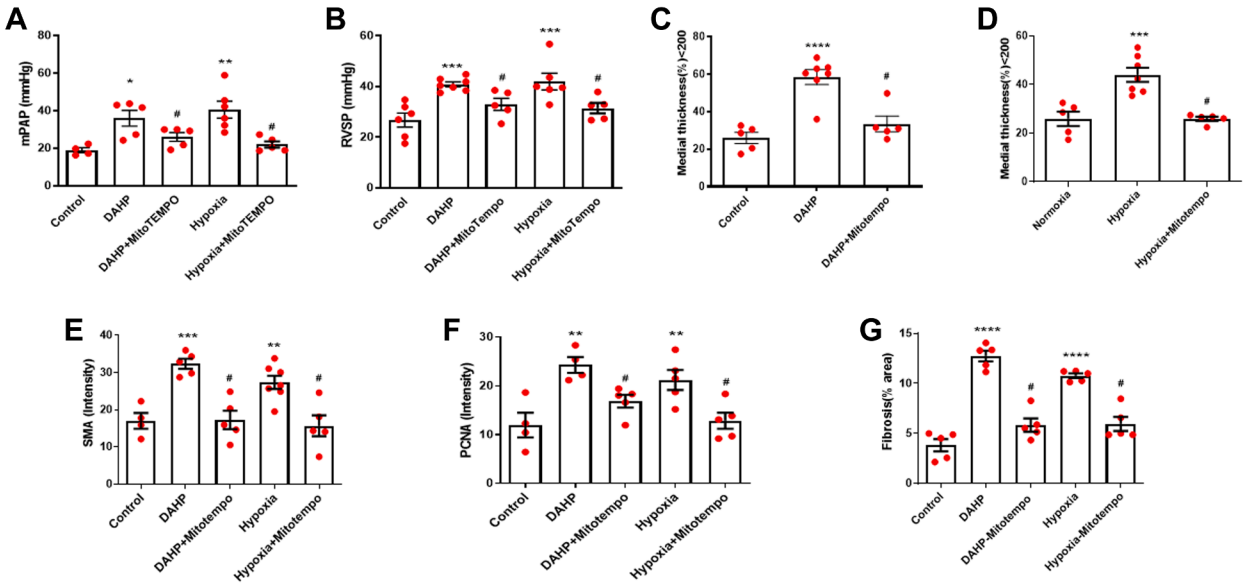

PH was induced by DAHP (10 mmol/L) or hypoxia (normobaric 10% O_2 and 5% CO_2 balanced with N_2) for 3 weeks, and some animals were treated with MitoTempo (dissolved in phosphate-buffered saline and used to treat mice daily at 0.7 mg/kg/d starting 2 days prior to DAHP/hypoxia treatment and throughout the entire treatment protocol). mPAP and RVSP were recorded by inserting 1.4-F catheter by open chest method using Power Lab data acquisition system. Changes are shown for mPAP (A) and RVSP (B) in both DAHP and hypoxia models. In parallel experiments, lung tissues were harvested after pressure measurement, fixed in para-formaldehyde, sectioned, and stained for H&E. (C,D) Grouped data for medial thickness indicating that MitoTempo treatment attenuated medial hypertrophy in arteries <200 μm in outer diameter size in both DAHP- and hypoxia-induced PH mice. (E) Quantitative data of fluorescent intensities of SMA. (F) Quantitative data of fluorescent intensities of PCNA expression. (G) Quantitative data of fibrosis. All data are expressed as mean ± SEM, n = 4-8 each. Data were analyzed by 1-way analysis of variance for multigroup comparison that was followed by Dunnet multiple comparison test. *P < 0.05 vs control group; **P < 0.001 vs control group; ***P < 0.001 vs control group; ****P < 0.0001 vs control group; #P < 0.05 vs DAHP or hypoxia groups. Abbreviations as in Figures 1 and 2.

with MitoTempo substantially attenuated vascular remodeling induced by hypoxia (12.85 ± 1.65).

Percentage fibrosis was determined by Masson trichrome staining. As shown in Figure 9G, fibrosis was significantly increased in DAHP group compared to control (12.74 ± 0.53 vs 3.82 ± 0.61 for DAHP vs control groups). Treatment with MitoTempo substantially attenuated vascular remodeling induced by DAHP (5.83 ± 0.66). Similarly, fibrosis was significantly increased in hypoxia group compared to control (10.77 ± 0.24 vs 3.82 ± 0.61 for hypoxia vs control groups). Treatment with MitoTempo also substantially attenuated vascular remodeling induced by hypoxia (5.95 ± 0.71).

Of note, treatment with MitoTempo also markedly suppressed superoxide production, compared to data in mice exposed to DAHP or hypoxia alone (Figures 10A and 10B). MitoSOX staining indicate that MitoTempo effectively abrogated mitochondrial ROS production in both DAHP and hypoxic models (Figure 10C). DAHP treatment significantly increased MitoSOX fluorescent intensity compared to control group (43.98 ± 2.85, n = 12 vs 26.74 ± 1.69, n = 10 for DAHP vs control groups). MitoTempo effectively attenuated MitoSOX fluorescent intensity induced by DAHP (28.15 ± 2.05, n = 10 vs 43.98 ± 2.85, n = 12 for DAHP + MitoTempo vs DAHP). Hypoxia exposure also increased MitoSOX fluorescent intensity compared to control group (51.14 ± 5.72, n = 12 vs 26.74 ± 1.69, n = 10 for hypoxia vs control groups). MitoTempo treatment also significantly alleviated MitoSOX fluorescent intensity induced by hypoxia (24.01 ± 1.65, n = 10 vs 51.14 ± 5.72, n = 12 for hypoxia + MitoTempo vs hypoxia).

In addition, we examined effects of MitoTempo on NO bioavailability. As shown in Figure 10D, MitoTempo treatment significantly recoupled eNOS and restored NO bioavailability. Whereas DAHP administration significantly decreased DAF-FM fluorescent intensity compared to control group (53.82 ± 5.38, n = 5 vs 25.32 ± 2.78, n = 7 for DAHP vs control groups), MitoTempo effectively restored DAF-FM

FIGURE 10 In vivo MitoTempo Treatment Attenuated Mitochondrial ROS Production While Restoring NO Bioavailability in Both DAHP- and Hypoxia-induced PH Mice

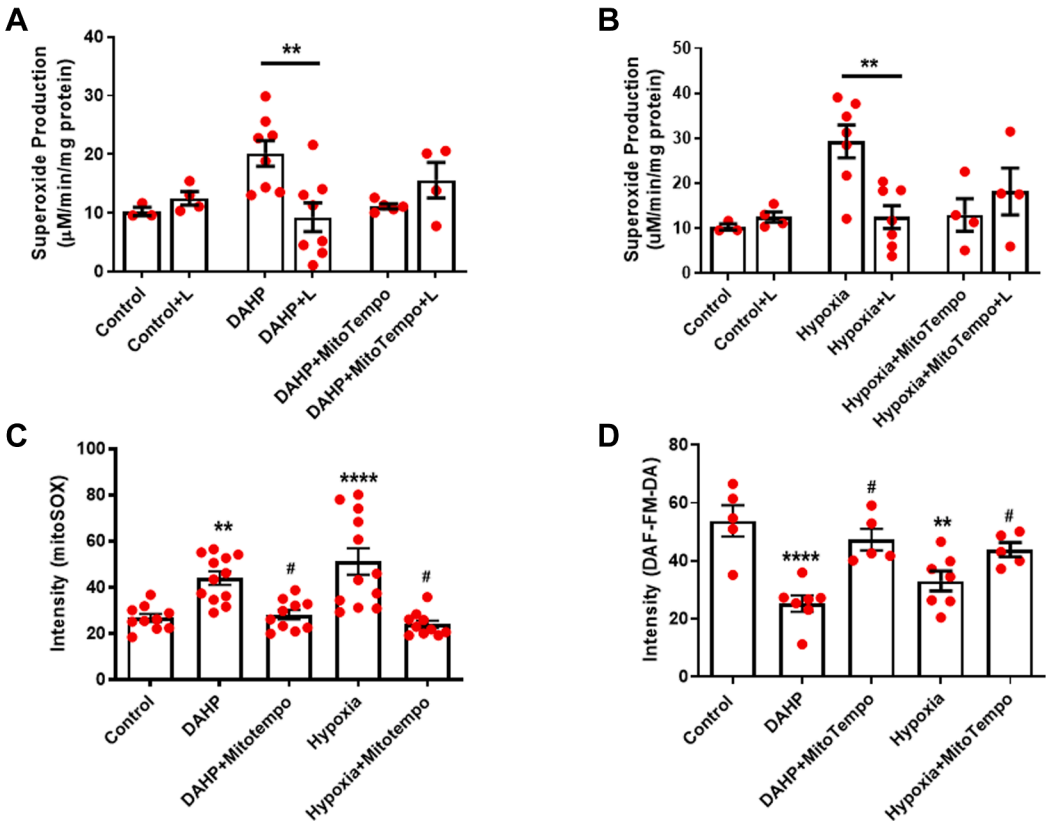

PH was induced by DAHP (10 mmol/L) or hypoxia (normobaric 10% O_2 and 5% CO_2 balanced with N_2) for 3 weeks, and some animals were treated with MitoTempo (dissolved in phosphate-buffered saline and used to treat mice daily at 0.7 mg/kg/d starting 2 days prior to DAHP/hypoxia treatment and throughout the entire treatment protocol). Total superoxide production measured from lung homogenates using electron spin resonance (ESR). eNOS uncoupling activity was assessed by comparing measurements with and without the addition of L-NAME, a NOS inhibitor. A reduction in superoxide production with L-NAME indicates that NOS is uncoupled and producing superoxide, whereas an increase in superoxide production with L-NAME indicates that NOS is coupled and producing NO. (A) Superoxide production measured from lung using ESR in DAHP + MitoTempo mice compared with mice treated with DAHP and control mice. (B) Superoxide production measured from lung using ESR in hypoxia + MitoTempo mice compared with mice exposed to hypoxia (normobaric 10% O_2 and 5% CO_2 balanced with 90% N_2) and control mice. Freshly harvested lung tissues were embedded in optimal cutting temperature compound, sectioned, and stained immediately with MitoSOX for mitochondrial ROS production and DAF-FM, which is a specific fluorescent probe for intracellular NO. (C) Grouped data for MitoSOX. (D) Grouped data for DAF-DM DA. All data are expressed as mean ± SEM, n = 5-10 each. Data were analyzed by 1-way analysis of variance for multigroup comparison that was followed by Dunnet multiple comparison test. $^{**}P < 0.001$ vs control group; $^{***}P < 0.001$ vs control group; $^{****}P < 0.0001$ vs control group; #$P < 0.05$ vs. DAHP or hypoxia groups. Abbreviations as in Figures 1, 4, and 5.

fluorescent intensity (47.35 ± 3.72, n = 5 vs 25.32 ± 2.78, n = 7 for DAHP + MitoTempo vs DAHP). Hypoxia exposure significantly reduced DAF-FM fluorescent intensity compared to control group (33.06 ± 3.45, n = 7 vs 53.82 ± 5.38, n = 5 for hypoxia vs control groups), and MitoTempo effectively recovered DAF-FM fluorescent intensity (43.88 ± 2.47, n = 5 vs. 33.06 ± 3.45, n = 7 for hypoxia + MitoTempo vs hypoxia) indicating restored NO bioavailability. Of note, feed-forward regulation of mitochondrial ROS further sustains eNOS uncoupling, whereas scavenging of mitochondrial ROS is effective in attenuating oxidative stress to improve NO bioavailability.

DAHP INDUCED eNOS UNCOUPLING, ER STRESS, AND MITOCHONDRIAL ROS GENERATION IN PAECs. We hypothesized that DAHP uncoupling of eNOS induces ER stress and mitochondrial dysfunction to result in persistent oxidative stress to cause

FIGURE 11 DAHP Treatment of PAECs Resulted in Increased Total and Mitochondrial Superoxide Production and eNOS Uncoupling Activity

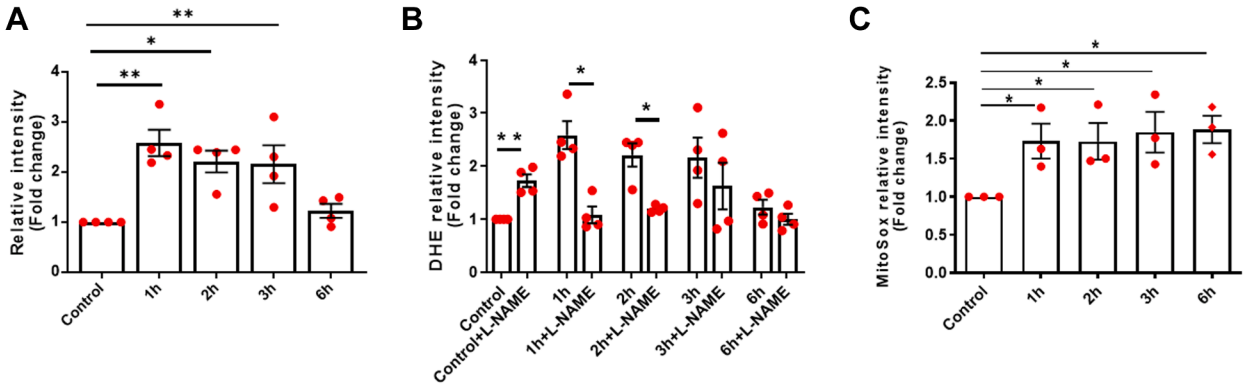

PAECs were treated with DAHP (5 mmol/L) for 1, 2, 3, and 6 hours prior to determination of total superoxide and mitochondrial superoxide production using DHE fluorescent imaging and MitoSOX imaging and quantitation. (A) Total superoxide production by DHE imaging and quantitation indicating rapid increase in superoxide production in PAECs treated with DAHP. (B) Superoxide production in the presence and absence of NOS inhibitor L-NAME, indicating eNOS uncoupling activity in DAHP-treated PAECs as soon as 1 hour after. (C) Mitochondrial superoxide production indicating increased and persistent elevation in mitochondrial superoxide production through 6 hours. All data are expressed as mean ± SEM, n = 3-4. Data were analyzed by 1-way analysis of variance for multigroup comparison that was followed by Newman-Keuls multiple comparison test. *$P < 0.05$, **$P < 0.01$. Abbreviations as in Figures 1-4 and 11.

remodeling of small pulmonary arteries, and that this response is initiated in the endothelial cells. To test this hypothesis, 1 day postconfluent PAECs were treated with DAHP (5 mmol/L) for 1, 2, 3, and 6 hours prior to DHE and MitoSOX determination of total ROS production and mitochondrial-derived ROS production. The induction of ER stress in PAECs exposed to DAHP was also determined by examining protein expression of PDI, an established marker for ER stress. As shown in Figure 11A, DAHP treatment induced eNOS uncoupling activity as measured by ROS production in the presence or absence of L-NAME. The measurements made without L-NAME indicate that DAHP treatment for 1, 2, and 3 hours significantly increased production of superoxide in comparison to control cells. The measurements made with L-NAME were done to assess the uncoupling state of eNOS. There was substantially increased eNOS uncoupling activity in DAHP-treated PAECs, especially at 1 and 2 hours (Figure 11B). Furthermore, mitochondrial superoxide production was also significantly up-regulated (Figure 11C), indicating downstream role of mitochondrial oxidative stress following eNOS uncoupling in DAHP-treated PAECs.

Taken together, our data establish a novel signaling axis of eNOS uncoupling/ER stress/mitochondrial dysfunction in the development of PH in both DAHP and hypoxia models. Upon DAHP or hypoxia exposure, eNOS uncoupling occurs, leading to downstream activation of ER stress and mitochondrial dysfunction, as well as persistent oxidative stress and consequent vascular remodeling to result in development of PH (Figure 12). Recoupling of eNOS with FA, suppression of ER stress by 4-PBA, or preservation of mitochondrial function with MitoTempo attenuated phenotypes and pathophysiological features of PH in both DAHP and hypoxic models. ROS production from stressed ER and dysfunctional mitochondria further sustains eNOS uncoupling activity; however, abrogation of this feed-back mechanism is effective in shutting down eNOS uncoupling activity to effectively abrogate development of PH (Figure 12)

DISCUSSION

The most significant finding of the present study is the first identification of a novel role of eNOS uncoupling/ER stress/mitochondrial dysfunction signaling axis in the development of PH in both novel and classic models of PH. Uncoupling of eNOS following DAHP or hypoxia stimulation leads to downstream activation of ER stress and mitochondrial dysfunction, as well as a feed-forward activation of eNOS uncoupling by ER stress and dysfunctional mitochondria, resulting in sustained oxidative stress, vascular remodeling, and all of molecular and pathophysiological features of PH. Recoupling of eNOS with FA, suppression of ER stress by 4-PBA, or preservation of mitochondrial function

FIGURE 12 An Innovative eNOS Uncoupling/ER Stress/Mitochondrial Dysfunction Cascade in Mediating Development of PH

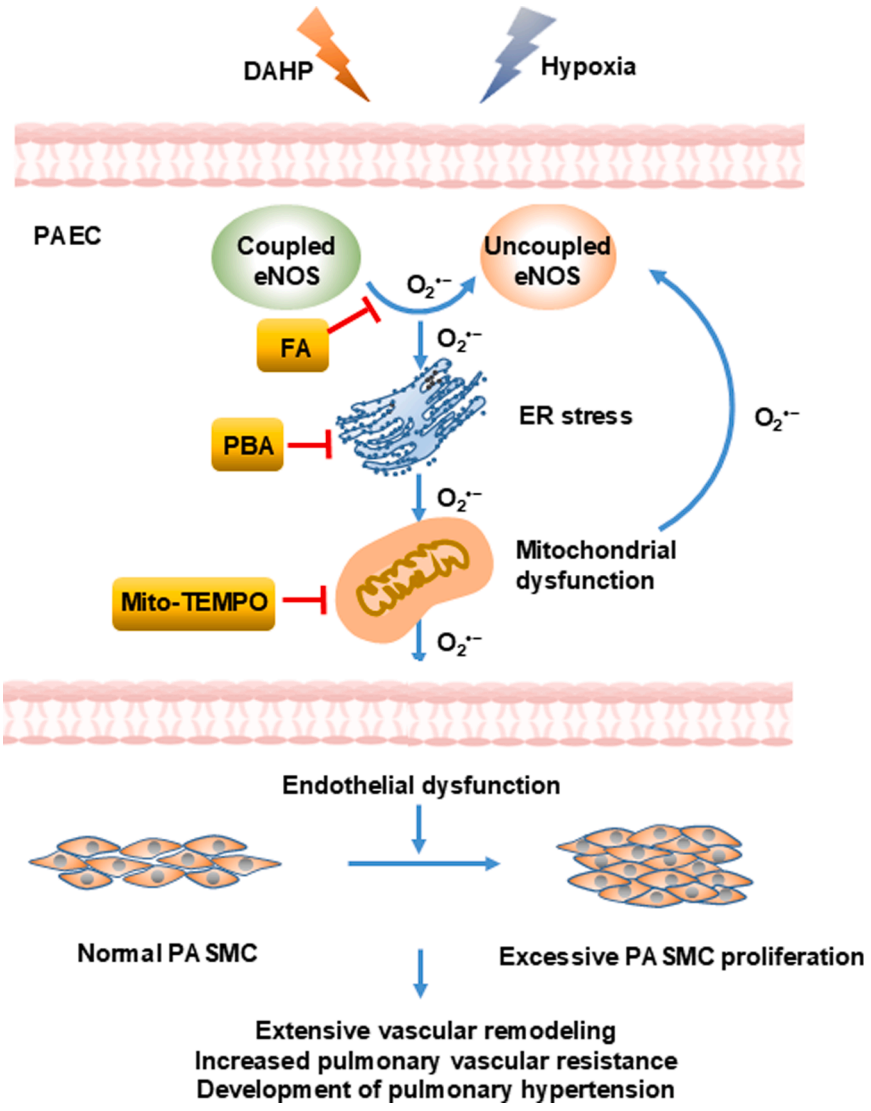

Under DAHP or hypoxia exposure, eNOS in the pulmonary arterial endothelial cells (PAECs) gets uncoupled to produce superoxide, which leads to consequent ER stress and subsequent mitochondrial dysfunction to proceed persistent endothelial dysfunction and a vicious cycle of superoxide production and oxidative stress. This cascaded events will induce vascular smooth muscle proliferation and vascular remodeling of increased medial thickness, resulting in increased pulmonary vascular resistance and development of PH. SMC = smooth muscle cell; other abbreviations as in Figures 1, 3, and 4.

with MitoTempo to specifically target mitochondrial ROS, completely attenuated molecular and pathophysiological features of PH in both DAHP and hypoxic models. In vitro, DAHP induced eNOS uncoupling, ER stress, and mitochondrial dysfunction in PAECs. Of note, severe mitochondrial dysfunction was observed in both DAHP and hypoxia models of PH as reflected by increased mitochondrial ROS production, increased calcium-induced swelling activity, and EM-defined disorganization of mitochondrial cristae. These data indicate that targeting eNOS uncoupling/ER stress/mitochondrial dysfunction signaling axis with pharmacologic inhibitors might prove to be innovative therapeutic strategies for the treatment of PH. It is of particular benefit for patients suffering from idiopathic PH and secondary PH. This is because the DAHP model directly targets the endothelium to induce endothelial dysfunction

that represents an initiating factor for idiopathic PH, whereas the hypoxia model represents a classic model of secondary PH.

Our data indicate that uncoupled eNOS contributes to development of PH in both DAHP and hypoxia models. Attenuation of eNOS uncoupling and ER stress with FA, PBA, and combinatory treatment abrogated PH in both DAHP and hypoxia models. Under physiological conditions, NO is produced in the vasculature by eNOS. Endothelial NO relaxes blood vessels, inhibits platelet activity, and protects against atherosclerosis. In the pulmonary vasculature, NO maintains vascular hemostasis to mediate vasodilatation and protect against vascular remodeling and thrombi formation. Under pathologic conditions such as hypercholesterolemia, hypertension, aortic aneurysms, and diabetes, eNOS becomes uncoupled when its key cofactor tetrahydrobiopterin is oxidized and deficient. Uncoupled eNOS generates superoxide instead of NO to substantially sustain oxidative stress, resulting in endothelial dysfunction. Reversal of eNOS uncoupling may represent a feasible strategy for the treatment of cardiovascular diseases.[46] Whereas uncoupled eNOS has been implicated in the pathogenesis of PH,[47-49] a direct causal role of eNOS uncoupling in PH development and its mechanistic downstream effectors have not been examined previously. Our previous study has shown that eNOS uncoupling activity lies upstream of mitochondrial dysfunction in the development of hypertension and abdominal aortic aneurysm.[26] In the present study, we identified a novel eNOS uncoupling/ER stress/mitochondrial dysfunction signaling axis in mediating PH development in both novel and classical models of PH. It is important to point out that our studies emphasize on a novel endothelial signaling cascade important for the development of PH, targeting of which represents new therapeutic directions. Whereas the role of endothelial dysfunction as the primary cause of idiopathic PAH has been established, our data provide compelling evidence on the mechanistic details that can be more efficiently targeted or intervened.

The present study aimed to examine whether ER stress and dysfunctional mitochondria, play important roles in PH development following uncoupling of eNOS. ER has been recognized as a principal organizer of cellular stress responses.[17] ER stress signaling in the pulmonary circulation involves activation of transcription factor 6, through the induction of the reticulin protein Nogo. This can disrupt the functional ER-mitochondria unit and cancer-like metabolic shift in pulmonary arterial hypertension that promotes proliferation and resistance to apoptosis in the pulmonary artery wall.[50] Recently published studies indicate that chemical chaperones like 4-PBA, which is known to suppress ER stress signaling, will inhibit the disruption of the ER-mitochondrial unit and prevent/reverse PH.[20,50,51] In the present study, we demonstrated a downstream role of ER stress following eNOS uncoupling to mediate development of PH in both DAHP and hypoxia stimulated PH models. ER stress lies downstream of uncoupled eNOS; and that inhibition of ER stress by PBA-alleviated molecular and pathophysiological features of PH in both DAHP and hypoxia models, firmly establishing an intermediate role of ER stress in PH development as a downstream effector of eNOS uncoupling. In addition, recoupling of eNOS with FA attenuated expression of ER stress marker PDI in lung tissue sections, indicating that eNOS activation mediated ER stress in both hypoxia- and DAHP-induced PH. PDI expression was also increased in DAHP-treated PAECs following DAHP administration to uncouple eNOS. Further, our present data clearly indicate that there was substantially increased eNOS uncoupling activity in DAHP-treated PAECs. Following treatment with DAHP, protein levels of PDI were significantly increased in PAECs, indicating downstream role of ER stress following eNOS uncoupling. Therefore, we believe that hydrogen peroxide produced by eNOS uncoupling/ER stress/mitochondrial dysfunction axis would then diffuse to underneath vascular smooth muscle cell to result in proliferation, migration, and other events involved in vascular remodeling.

Mitochondria control apoptosis and produce reactive oxygen species like H_2O_2, which can regulate vascular tone via activation of K^+ channels, but their role in the pathogenesis of PH is incompletely understood. Studies have identified dichloroacetate, a metabolic modulator that increases mitochondrial oxidative phosphorylation, prevents and reverses monocrotaline-induced PH. The vascular smooth muscle cells that proliferate during progression of PH are characterized by mitochondrial hyperpolarization, activation of the transcription factor NFAT, and down-regulation of the voltage-gated potassium channel Kv1.5, all of which suppress apoptosis. Another study revealed that deletion of the metabolic enzyme malonyl-coenzyme A decarboxylase results in an inhibition of fatty acid oxidation, which in turn promotes glucose oxidation and prevents the shift in metabolism toward glycolysis in pulmonary

blood vessels, which drives the development of PH.[52-54] PH pathogenesis, much like in cancer, is featured by a switch to aglycolytic phenotype that promotes proliferation while suppressing apoptosis,[54,55] which can in turn contribute to vascular remodeling and formation of vascular lesions. Our data showed that treatment with to scavenge mitochondrial ROS completely attenuated molecular and pathophysiological features of PH in both DAHP and hypoxia models, indicating a role of mitochondrial dysfunction in PH development. In addition, calcium-induced mitochondrial swelling activity was markedly increased in DAHP- or hypoxia-treated mice, which was abrogated by treatment with FA or PBA, indicating upstream roles of uncoupled eNOS and ER stress in inducing mitochondrial dysfunction in the pathogenesis of PH. In this study, we also report severe mitochondrial dysfunction in both hypoxia and DAHP models of PH, which was reflected by swollen mitochondria, disorganized mitochondrial cristae, and increased mitochondrial ROS generation.

Importantly, our findings have great translational potential and promptness, because FA and PBA are both US Food and Drug Administration-approved drugs for other medical conditions. FA is used as a nutrition supplement for pregnant women to prevent neural tube defects, and 4-PBA has been used as a medication for urea cycle disorders, a genetic condition characterized by excessive ammonia in the blood. Therefore, these drugs can be quickly repurposed for the treatment of PH with the convenience of known toxicity profiles, potential dosing, and possible side effects. Our new observations revealing mechanistic details whereby these medications are on target to be beneficial in treating PH, will no doubt facilitate rapid translational adaptation to clinical practice to generate new therapies for PH that would be effective in alleviating pathophysiological processes of the disease but not just the clinical symptoms, which is necessary to stop disease progression to save lives.

CONCLUSIONS

The present study identified a novel eNOS uncoupling/ER stress/mitochondrial dysfunction signaling axis in mediating PH development in both novel and classical models of PH. Aggravated eNOS uncoupling activity induces ER stress and subsequent mitochondrial dysfunction, contributing to the development of PH. In vivo, the inhibitors targeting eNOS uncoupling/ER stress/mitochondrial dysfunction axis are completely effective in abolishing phenotypes of PH. Interestingly, treatment with FA to recouple eNOS, or with PBA to preserve ER function, resulted in decreased mPAP and RVSP, attenuated vascular remodeling, abrogated total and mitochondrial superoxide production and eNOS uncoupling activity, and diminished mitochondrial swelling activity while preserving NO bioavailability, reduced ER stress marker PDI expressions in both DAHP-treated or hypoxia-exposed animals. In addition, treatment with MitoTempo to scavenge mitochondrial ROS completely attenuated molecular and pathophysiological features of PH in both DAHP and hypoxia models, indicating a role of mitochondrial dysfunction in PH development. the eNOS uncoupling/ER stress/mitochondrial dysfunction axis may therefore prove to be a novel therapeutic option for the treatment of PH.

ACKNOWLEDGMENTS The authors of Dr Priya Murugesan, Dr Yunxian Zhang, Dr Meng Zhang and Dr Yixuan Zhang all have made substantial contributions to this work. Due to restriction to list two co-first authors by journal policy, the first two co-first authors Dr Priya Murugesan and Dr Yunxia Zhang are denoted as such based on extents of contributions, whereas Dr Meng Zhang and Dr Yixuan Zhang are also considered co-first authors on this work

FUNDING SUPPORT AND AUTHOR DISCLOSURES

This work was supported by the National Heart, Lung, and Blood Institute grants HL077440 (to H.C.), HL088975 (to H.C.), HL142951 (to H.C.), HL154754 (to H.C. and A.M.), and HL162407 (to H.C. and J.G.). The authors have reported that they have no relationships relevant to the contents of this paper to disclose.

ADDRESS FOR CORRESPONDENCE: Dr Hua Cai, Division of Molecular Medicine, Department of Anesthesiology, Division of Cardiology, Department of Medicine, David Geffen School of Medicine, University of California Los Angeles, Los Angeles, California, 90095, USA. E-mail: hcai@mednet.ucla.edu.

PERSPECTIVES

CLINICAL COMPETENCY: COMPETENCY IN MEDICAL KNOWLEDGE: Our novel and robust findings reveal new mechanistic insights into pathogenesis of PH, targeting of which will no doubt facilitate rapid development of novel therapeutics. Our data identified an important signaling axis of eNOS uncoupling/ER stress/mitochondrial dysfunction that mediates vascular remodeling and vascular lesion formation in PH. These represent innovative new medical knowledge to be leveraged for the design of treatment options for PH.

TRANSLATIONAL OUTLOOK: Our findings have great and immediate translational outlook, because FA and PBA are both US Food and Drug Administration–approved drugs for other medical conditions. These drugs can be quickly repurposed for the treatment of PH with the convenience of known toxicity profiles, potential dosing, and possible side effects. Our new observations revealing mechanistic details whereby these medications are on target to be beneficial in treating PH, will promote rapid translational adaptation to clinical practice, to generate new therapies that would be effective in alleviating pathophysiological processes of the disease but not just the clinical symptoms, which is necessary to stop disease progression to save lives.

REFERENCES

1. Tonelli AR, Arelli V, Minai OA, et al. Causes and circumstances of death in pulmonary arterial hypertension. *Am J Respir Crit Care Med*. 2013;188(3):365-369. https://doi.org/10.1164/rccm.201209-1640OC

2. Simonneau G, Montani D, Celermajer DS, et al. Haemodynamic definitions and updated clinical classification of pulmonary hypertension. *Eur Respir J*. 2019;53(1):1801913. https://doi.org/10.1183/13993003.01913-2018

3. Galiè N, Humbert M, Vachiery JL, et al. 2015 ESC/ERS Guidelines for the diagnosis and treatment of pulmonary hypertension: the Joint Task Force for the Diagnosis and Treatment of Pulmonary Hypertension of the European Society of Cardiology (ESC) and the European Respiratory Society (ERS): endorsed by: Association for European Paediatric and Congenital Cardiology (AEPC), International Society for Heart and Lung Transplantation (ISHLT). *Eur Respir J*. 2015;46(4):903-975. https://doi.org/10.1183/13993003.01032-2015

4. Gali N, Palazzini M, Manes A. Pulmonary arterial hypertension: from the kingdom of the near-dead to multiple clinical trial meta-analyses. *Eur Heart J*. 2010;31(17):2080-2086. https://doi.org/10.1093/eurheartj/ehq152

5. Humbert M, Sitbon O. Treatment of pulmonary arterial hypertension. *New Engl J Med*. 2004;351(14):1425-1436. https://doi.org/10.1056/NEJMra040291

6. Jaitovich A, Jourd'heuil D. A brief overview of nitric oxide and reactive oxygen species signaling in hypoxia-induced pulmonary hypertension. *Adv Exp Med Biol*. 2017;967:71-81. https://doi.org/10.1007/978-3-319-63245-2_6

7. Klinger JR, Kadowitz PJ. The nitric oxide pathway in pulmonary vascular disease. *Am J Cardiol*. 2017;120(8S):S71-S79. https://doi.org/10.1016/j.amjcard.2017.06.012

8. Barst RJ, Channick R, Ivy D, Goldstein B. Clinical perspectives with long-term pulsed inhaled nitric oxide for the treatment of pulmonary arterial hypertension. *Pulm Circ*. 2012;2(2):139-147. https://doi.org/10.4103/2045-8932.97589

9. Konduri GG, Menzin J, Frean M, Lee T, Potenziano J, Singer J. Inhaled nitric oxide in term/late preterm neonates with hypoxic respiratory failure: estimating the financial impact of earlier use. *J Med Econ*. 2015;18(8):612-618. https://doi.org/10.3111/13696998.2015.1038270

10. Francis SH, Busch JL, Corbin JD. cGMP-dependent protein kinases and cGMP phosphodiesterases in nitric oxide and cGMP action. *Pharmacol Rev*. 2010;62(3):525-563. https://doi.org/10.1124/pr.110.002907

11. Ghofrani H-A, Galiè N, Grimminger F, et al. Riociguat for the treatment of pulmonary arterial hypertension. *N Engl J Med*. 2013;369(4):330-340. https://doi.org/10.1056/nejmoa1209655

12. Rubin LJ, Galié N, Grimminger F, et al. Riociguat for the treatment of pulmonary arterial hypertension: a long-term extension study (patent-2). *Eur Respir J*. 2015;45(5):1303-1313. https://doi.org/10.1183/09031936.00090614

13. Ghofrani HA, Grimminger F, Grünig E, et al. Predictors of long-term outcomes in patients treated with riociguat for pulmonary arterial hypertension: data from the PATENT-2 open-label, randomised, long-term extension trial. *Lancet Respir Med*. 2016;4(5):361-371. https://doi.org/10.1016/S2213-2600(16)30019-4

14. McLaughlin V, Channick RN, Ghofrani HA, et al. Bosentan added to sildenafil therapy in patients with pulmonary arterial hypertension. *Eur Respir J*. 2015;46(2):405-413. https://doi.org/10.1183/13993003.02044-2014

15. Johnson SR, Brode SK, Mielniczuk LM, Granton JT. Dual therapy in IPAH and SSc-PAH: a qualitative systematic review. *Respir Med*. 2012;106(5):730-739. https://doi.org/10.1016/j.rmed.2011.12.018

16. Murugesan P, Zhang Y, Huang Y, et al. Reversal of pulmonary hypertension in a human-like model: therapeutic targeting of endothelial DHFR. *Circ Res*. 2024;134(4):351-370.

17. Ochoa CD, Wu RF, Terada LS. ROS signaling and ER stress in cardiovascular disease. *Mol Aspects Med*. 2018;63:18-29. https://doi.org/10.1016/j.mam.2018.03.002

18. Münzel T, Camici GG, Maack C, Bonetti NR, Fuster V, Kovacic JC. Impact of oxidative stress on the heart and vasculature: part 2 of a 3-part series. *J Am Coll Cardiol*. 2017;70(2):212-229. https://doi.org/10.1016/j.jacc.2017.05.035

19. Tse G, Yan BP, Chan YWF, Tian XY, Huang Y. Reactive oxygen species, endoplasmic reticulum stress and mitochondrial dysfunction: the link with cardiac arrhythmogenesis. *Front Physiol*. 2016;7:313. https://doi.org/10.3389/fphys.2016.00313

20. Koyama M, Furuhashi M, Ishimura S, et al. Reduction of endoplasmic reticulum stress by 4-phenylbutyric acid prevents the development of hypoxia-induced pulmonary arterial hypertension. *Am J Physiol Heart Circ Physiol*. 2014;306(9):H1314-H1323. https://doi.org/10.1152/ajpheart.00869.2013

21. Liu Y, Wang Y, Ding W, Wang Y. Mito-TEMPO alleviates renal fibrosis by reducing inflammation, mitochondrial dysfunction, and endoplasmic reticulum stress. *Oxid Med Cell Longev*. 2018;2018:5828120. https://doi.org/10.1155/2018/5828120

22. Tompkins AJ, Burwell LS, Digerness SB, Zaragoza C, Holman WL, Brookes PS. Mitochondrial dysfunction in cardiac ischemia-reperfusion injury: ROS from complex I, without inhibition. *Biochim Biophys Acta*. 2006;1762(2):223-231. https://doi.org/10.1016/j.bbadis.2005.10.001

23. Guignabert C, Phan C, Seferian A, et al. Dasatinib induces lung vascular toxicity and predisposes to pulmonary hypertension. *J Clin Invest*. 2016;126(9):3207-3218. https://doi.org/10.1172/JCI86249

24. Adesina SE, Kang BY, Bijli KM, et al. Targeting mitochondrial reactive oxygen species to modulate hypoxia-induced pulmonary hypertension. *Free Radic Biol Med*. 2015;87:36-47. https://doi.org/10.1016/j.freeradbiomed.2015.05.042

25. Culley MK, Chan SY. Mitochondrial metabolism in pulmonary hypertension: beyond mountains there are mountains. *J Clin Invest*. 2018;128(9):3704-3715. https://doi.org/10.1172/JCI120847

26. Li Q, Youn JY, Siu KL, Murugesan P, Zhang Y, Cai H. Knockout of dihydrofolate reductase in mice induces hypertension and abdominal aortic aneurysm via mitochondrial dysfunction. *Redox Biol*. 2019;24:101185. https://doi.org/10.1016/j.redox.2019.101185

27. Chen Q, Thompson J, Hu Y, Das A, Lesnefsky EJ. Metformin attenuates ER stress-induced mitochondrial dysfunction. *Transl Res*. 2017;190:40-50. https://doi.org/10.1016/j.trsl.2017.09.003

28. Gao L, Siu KL, Chalupsky K, et al. Role of uncoupled endothelial nitric oxide synthase in abdominal aortic aneurysm formation: treatment with folic acid. *Hypertension*. 2012;59(1):158-166. https://doi.org/10.1161/HYPERTENSIONAHA.111.181644

29. Li Q, Yon J-Y, Cai H. Mechanisms and consequences of eNOS dysfunction in hypertension. *J Hypertens*. 2015;33(6):1128-1136. https://doi.org/10.1097/HJH.0000000000000587

30. Oak JH, Cai H. Attenuation of angiotensin II signaling recouples eNOS and inhibits non-endothelial NOX activity in diabetic mice. *Diabetes*. 2007;56(1):118-126. https://doi.org/10.2337/db06-0288

31. Gao L, Chalupsky K, Stefani E, Cai H. Mechanistic insights into folic acid-dependent vascular protection: dihydrofolate reductase (DHFR)-mediated reduction in oxidant stress in endothelial cells and angiotensin II-infused mice: a novel HPLC-based fluorescent assay for DHFR activity. *J Mol Cell Cardiol*. 2009;47(6):752-760. https://doi.org/10.1016/j.yjmcc.2009.07.025

32. Youn JY, Gao L, Cai H. The p47phox-and NADPH oxidase organiser 1 (NOXO1)-dependent activation of NADPH oxidase 1 (NOX1) mediates endothelial nitric oxide synthase (eNOS) uncoupling and endothelial dysfunction in a streptozotocin-induced murine model of diabetes. *Diabetologia*. 2012;55(7):2069-2079. https://doi.org/10.1007/s00125-012-2557-6

33. Siu KL, Lotz C, Ping P, Cai H. Netrin-1 abrogates ischemia/reperfusion-induced cardiac mitochondrial dysfunction via nitric oxide-dependent attenuation of NOX4 activation and recoupling of NOS. *J Mol Cell Cardiol*. 2015;78:174-185. https://doi.org/10.1016/j.yjmcc.2014.07.005

34. Siu KL, Cai H. Circulating tetrahydrobiopterin as a novel biomarker for abdominal aortic aneurysm. *Am J Physiol Circ Physiol*. 2014;307(11):H1559-H1564. https://doi.org/10.1152/ajpheart.00444.2014

35. Moens AL, Kass DA. Tetrahydrobiopterin and cardiovascular disease. *Arterioscler Thromb Vasc Biol*. 2006;26(11):2439-2444. https://doi.org/10.1161/01.ATV.0000243924.00970.cb

36. Chalupsky K, Cai H. Endothelial dihydrofolate reductase: critical for nitric oxide bioavailability and role in angiotensin II uncoupling of endothelial nitric oxide synthase. *Proc Natl Acad Sci U S A*. 2005;102(25):9056-9061. https://doi.org/10.1073/pnas.0409594102

37. Siu KL, Miao XN, Cai H. Recoupling of eNOS with folic acid prevents abdominal aortic aneurysm formation in angiotensin II-infused apolipoprotein E null mice. *PLoS One*. 2014;9(2):e88899. https://doi.org/10.1371/journal.pone.0088899

38. Zhang J, Cai H. Netrin-1 prevents ischemia/reperfusion-induced myocardial infarction via a DCC/ERK1/2/eNOSs1177/NO/DCC feed-forward mechanism. *J Mol Cell Cardiol*. 2010;48(6):1060-1070. https://doi.org/10.1016/j.yjmcc.2009.11.020

39. Bouhidel JO, Wang P, Siu KL, Li H, Youn JY, Cai H. Netrin-1 improves post-injury cardiac function in vivo via DCC/NO-dependent preservation of mitochondrial integrity, while attenuating autophagy. *Biochim Biophys Acta*. 2015;1852(2):277-289. https://doi.org/10.1016/j.bbadis.2014.06.005

40. Youn J, Siu KL, Lob HE, Itani H, Harrison DG, Cai H. Role of vascular oxidative stress in obesity and metabolic syndrome. *Diabetes*. 2014;63(7):2344-2355. https://doi.org/10.2337/db13-0719

41. Chalupsky K, Kračun D, Kanchev I, Bertram K, Görlach A. Folic acid promotes recycling of tetrahydrobiopterin and protects against hypoxia-induced pulmonary hypertension by recoupling endothelial nitric oxide synthase. *Antioxid Redox Signal*. 2015;23(14):1076-1091. https://doi.org/10.1089/ars.2015.6329

42. Octavia Y, Kararigas G, de Boer M, et al. Folic acid reduces doxorubicin-induced cardiomyopathy by modulating endothelial nitric oxide synthase. *J Cell Mol Med*. 2017;21(12):3277-3287. https://doi.org/10.1111/jcmm.13231

43. Moens AL, Vrints CJ, Claeys MJ, Timmermans JP, Champion HC, Kass DA. Mechanisms and potential therapeutic targets for folic acid in cardiovascular disease. *Am J Physiol Heart Circ Physiol*. 2008;294(5):H1971-H1977. https://doi.org/10.1152/ajpheart.91503.2007

44. Stenmark KR, Meyrick B, Galie N, Mooi WJ, McMurtry IF. Animal models of pulmonary arterial hypertension: the hope for etiological discovery and pharmacological cure. *Am J Physiol Cell Mol Physiol*. 2009;297(6):L1013-L1032. https://doi.org/10.1152/ajplung.00217.2009

45. Rhodes J. Comparative physiology of hypoxic pulmonary hypertension: historical clues from brisket disease. *J Appl Physiol (1985)*. 2005;98(3):1092-1100. https://doi.org/10.1152/japplphysiol.01017.2004

46. Zhang Y, Murugesan P, Huang K, Cai H. NADPH oxidases and oxidase crosstalk in cardiovascular diseases: novel therapeutic targets. *Nat Rev Cardiol*. 2020;17(3):170-194. https://doi.org/10.1038/s41569-019-0260-8

47. Klinger JR, Abman SH, Gladwin MT. Nitric oxide deficiency and endothelial dysfunction in pulmonary arterial hypertension. *Am J Respir Crit Care Med*. 2013;188(6):639-646. https://doi.org/10.1164/rccm.201304-0686PP

48. Khoo JP, Zhao L, Alp NJ, et al. Pivotal role for endothelial tetrahydrobiopterin in pulmonary hypertension. *Circulation*. 2005;111(16):2126-2133. https://doi.org/10.1161/01.CIR.0000162470.26840.89

49. d'Uscio LV. ENOS uncoupling in pulmonary hypertension. *Cardiovasc Res*. 2011;92(3):359-360. https://doi.org/10.1093/cvr/cvr270

50. Dromparis P, Paulin R, Stenson TH, Haromy A, Sutendra G, Michelakis ED. Attenuating endoplasmic reticulum stress as a novel therapeutic strategy in pulmonary hypertension. *Circulation*. 2013;127(1):115-125. https://doi.org/10.1161/CIRCULATIONAHA.112.133413

51. Dromparis P, Paulin R, Sutendra G, Qi AC, Bonnet S, Michelakis ED. Uncoupling protein 2 deficiency mimics the effects of hypoxia and endoplasmic reticulum stress on mitochondria and triggers pseudohypoxic pulmonary vascular remodeling and pulmonary hypertension. *Circ Res*. 2013;113(2):126-136. https://doi.org/10.1161/CIRCRESAHA.112.300699

52. McMurtry MS, Bonnet S, Wu X, et al. Dichloroacetate prevents and reverses pulmonary hypertension by inducing pulmonary artery smooth muscle cell apoptosis. *Circ Res*. 2004;95(8):830-840. https://doi.org/10.1161/01.RES.0000145360.16770.9f

53. Michelakis ED, McMurtry MS, Wu XC, et al. Dichloroacetate, a metabolic modulator, prevents and reverses chronic hypoxic pulmonary hypertension in rats: role of increased expression and activity of voltage-gated potassium channels. *Circulation*. 2002;105(2):244-250. https://doi.org/10.1161/hc0202.101974

54. Sutendra G, Bonnet S, Rochefort G, et al. Fatty acid oxidation and malonyl-CoA decarboxylase in the vascular remodeling of pulmonary hypertension. *Sci Transl Med*. 2010;2(44):44ra58. https://doi.org/10.1126/scitranslmed.3001327

55. Dromparis P, Sutendra G, Michelakis ED. The role of mitochondria in pulmonary vascular remodeling. *J Mol Med (Berl)*. 2010;88(10):1003-1010. https://doi.org/10.1007/s00109-010-0670-x

KEY WORDS 2,4-diamino 6-hydroxypyrimidine (DAHP), dihydrofolate reductase, endothelial dysfunction, eNOS uncoupling, ER stress, hypoxia, mitochondrial dysfunction, pulmonary hypertension, vascular remodeling